Th/U ratios in metamorphic zircon

Chris Yakymchuk[1,*], Christopher L. Kirkland[2], Chris Clark[2]

[1]Department of Earth and Environmental Sciences, University of Waterloo, Waterloo, Ontario, Canada,
N2L 3G1, *cyakymchuk@uwaterloo.ca

[2]Department of Applied Geology, Curtin University, Perth, Western Australia, Australia, 6102

ABSTRACT

The Th/U ratios of zircon crystals are routinely used to help understand their growth mechanism. Despite the wide application of Th/U ratios in understanding the geological significance of zircon U–Pb ages, the main controls on the Th/U ratio in metamorphic zircon are poorly understood. Here, phase equilibria modelling coupled with solubility expressions for accessory minerals are used to investigate the controls on the Th/U ratios of suprasolidus metamorphic zircon in an average amphibolite-facies metapelite composition. We also present a new database of metamorphic Th/U ratios in zircon from Western Australia. Several factors affecting the Th/U ratio are investigated, including the bulk rock concentrations of Th and U, the amount of monazite and apatite in the system, and open versus closed system behaviour. Our modelling predicts that the main controls on the Th/U ratio of suprasolidus metamorphic zircon are the concentrations of Th and U in the system and the breakdown and growth of monazite in equilibrium with zircon. Furthermore, the relative timing of zircon and monazite growth during cooling and melt crystallization has an important role in the Th/U ratio of zircon. Early grown zircon near the peak of metamorphism is expected to have elevated Th/U ratios whereas zircon that grew near the solidus is predicted to have relatively low Th/U ratios, which reflects the coeval growth of monazite during cooling and melt crystallization. Our modelling approach aims to provide an improved understanding of the main controls of Th/U in metamorphic zircon in migmatites and hence better apply this geochemical ratio as a tool to assist in interpretation of the genesis of metamorphic zircon.

KEY WORDS: zircon, Th/U, monazite, metamorphic, migmatite, phase equilibria

1 INTRODUCTION

Zircon U–Pb geochronology is a powerful tool in determining the absolute timing, duration and hence geodynamic significance of metamorphic events (Harley, Kelly, & Möller, 2007; Rubatto & Hermann, 2007; Rubatto, 2017). In igneous rocks, magmatic zircon grows during the crystallization of melt when the melt reaches saturation in Zr with respect to zircon (e.g. Boehnke, Watson, Trail, Harrison, & Schmitt, 2013). In metamorphic systems, zircon can grow or recrystallize at *P–T* conditions below the solidus (subsolidus metamorphic zircon) or crystallize from melt above the solidus (suprasolidus metamorphic zircon or anatectic zircon).

Zircon in igneous and metamorphic systems concentrates U and Th, which permits geochronological investigation and the concentration of these elements in zircon has potential to help elucidate the crystal's growth mechanism. Metamorphic rocks commonly contain multiple age populations of zircon that reflect both inherited and newly grown material, with the Th/U ratio used as a tool to distinguish between different populations (Hoskin & Schaltegger, 2003; Rubatto & Gebauer, 2000; Rubatto, 2002; Rubatto, 2017; Schaltegger et al., 1999; Williams & Claesson, 1987). A common observation is that most metamorphic zircon has Th/U ratios <0.1, except in high-temperature and ultrahigh-temperature (UHT) metamorphic rocks, where this ratio is frequently >0.1 (e.g. Harley et al., 2007; Kelley & Harley, 2005; Kelsey & Hand, 2015; Korhonen, Clark, Brown, Bhattacharya, & Taylor, 2013; Rubatto, 2017; Vavra, Schmid, & Gebauer, 1996). However, the reasons for this variation in zircon Th/U are not always clear.

An important control on the Th/U of zircon in metamorphic rocks may be the coeval growth of Th-rich accessory minerals, such as monazite and allanite (Harley et al., 2007; Kelsey & Hand, 2015; Kirkland, Smithies, Taylor, Evans, & McDonald, 2015; Schaltegger & Davies, 2017; Rubatto, 2017). Monazite and allanite are expected to be the dominant hosts of Th in metamorphic rocks whereas zircon, monazite, xenotime, apatite and allanite can share the majority of the U budget (Bea, 1996; Bea & Montero, 1999; Hermann, 2002). The major rock-forming minerals contain a relatively minor proportion of the Th and U in most metamorphic rocks. Therefore, the breakdown and growth of Th-rich (and to a lesser extent U-rich) accessory minerals will have a major effect on the Th/U ratios of equilibrated zircon.

Allanite is generally restricted to relatively high-Ca bulk compositions (Finger, Krenn, Schulz, Harlov, & Schiller, 2016; Wing, Ferry, & Harrison, 2003) and subsolidus conditions in metapelites (Spear & Pyle, 2010) whereas monazite is common in metapelites at subsolidus and suprasolidus conditions. Above the solidus, monazite is the dominant reservoir of Th (e.g. Bea & Montero, 1999) due to the large monazite–melt partition coefficient of Th relative to other minerals (e.g. Stepanov, Hermann, Rubatto, & Rapp, 2012). During high-temperature metamorphism and anatexis, monazite is expected to break down and hence saturate the anatectic melt in Light Rare Earth Elements (LREE). The suprasolidus behaviour of monazite is a function of temperature, pressure, melt chemistry, bulk composition (Duc-Tin & Keppler, 2015; Montel, 1986; Rapp & Watson, 1986; Rapp, Ryerson, & Miller, 1987; Skora & Blundy, 2012; Stepanov et al., 2012). The growth and breakdown of apatite also impacts the stability of monazite during anatexis (Johnson, Clark, Taylor, Santosh, & Collins, 2015; Yakymchuk, 2017).

When monazite is present in an equilibrated system it is expected to host a large proportion of the Th budget in the rock. Zircon in equilibrium with this monazite is expected to have relatively low Th/U ratios (e.g. Cesare, Gómez-Pugnaire, & Rubatto, 2003; Rubatto, Williams, & Buick, 2001; Rubatto, 2017; Vavra et al., 1996). If monazite becomes completely consumed during anatexis, zircon in equilibrium with the melt could be expected to have relatively high Th/U ratios unless there is an additional sink for Th. Therefore, in aluminous metasedimentary migmatites, one of the primary controls on the Th/U ratio of equilibrated zircon is thought to be the presence or absence of monazite. However, to our knowledge, no attempt has been made to quantitatively model the Th/U ratio of suprasolidus metamorphic zircon in monazite-buffered systems and to evaluate other possible reasons for the observed Th/U ratios in suprasolidus metamorphic zircon.

In this contribution, to provide context to our study we first present a database of Th/U ratios in metamorphic and igneous zircon from Western Australia to evaluate the range of values in metamorphic versus igneous zircon and show that a single threshold Th/U ratio is not always appropriate for distinguishing the origin of zircon. To evaluate why metamorphic zircon can record a spread in Th/U ratios, we then use forward phase equilibria modelling coupled with solubility equations for monazite, apatite and zircon in anatectic melt to investigate the controls on Th/U ratios of metamorphic zircon in a suprasolidus metapelite. We investigate several factors that can control Th/U ratios in suprasolidus metamorphic zircon grains, including bulk-rock compositions, variations in partition coefficients, and open-system behaviour. The modelling results presented here are generally applicable to suprasolidus metamorphism of metasedimentary rocks that contain an equilibrium assemblage with accessory monazite, zircon and apatite. Our findings have implications for interpreting Th/U ratios of zircon in high-temperature and UHT metamorphic rocks.

2 COMPILATION OF TH/U RATIOS IN METAMORPHIC ZIRCON

The range of Th/U ratios in metamorphic zircon can vary over several orders of magnitude (e.g. Harley et al., 2007; Hoskin & Schaltegger, 2003; Rubatto, 2017). To demonstrate the variability of Th/U ratios in natural samples and the difference between igneous and metamorphic zircon, a SIMS dataset of 1352 analyses of metamorphic zircon and 5794 analyses of igneous zircon from published geochronology results in Western Australia is summarized in Figure 1. The dataset for the metamorphic zircon group is presented in supplementary Table S1. Data for the igneous group are from the compilation in Kirkland et al. (2015). The data exclude analyses that have >10% U–Pb discordance in order to exclude metamict zircon. Analyses have been categorised based on all or some of the following: cathodoluminescence texture, isotopic date in relation to regional age patterns, lithology (e.g. metamorphosed versus unmetamorphosed), and information from other isotopic systems including oxygen and ^{176}Hf/^{177}Hf. All such interpretations of zircon growth (e.g. igneous or metamorphic) are published in the Geological

Survey of Western Australia geochronology record series (http://www.dmp.wa.gov.au/geochron). For the metamorphic zircon group, data include Archean, Proterozoic and Phanerozoic examples from the major metamorphic belts in Western Australia, including the Pilbara, Yilgarn, Albany–Fraser Orogen, Musgrave Province, Capricorn Orogen, Rudall Province as well as associated basins. The data record a wide variety of metamorphic conditions and suprasolidus and subsolidus metamorphic zircon are not distinguished.

The Th/U ratios of metamorphic zircon from Western Australia range from <0.001 to >10 (Figure 1a–d) and are highly skewed towards lower values (Figure 1a). The entire dataset yields a median value of 0.44 and values of 0.08 and 1.08 for the 25th and 75th percentiles, respectively. The distribution of the dataset is roughly log-normal (inset in Figure 1a), but the log-normalized dataset is also slightly skewed towards lower ratios of Th/U ratios in zircon.

Thorium and U concentrations in metamorphic zircon are highly skewed towards low values (Figure 1b, c). Concentrations of Th in zircon have a median value of 105 ppm and 25th and 75th percentile values of 28 ppm and 232 ppm, respectively. The log-normalized Th concentration data is also skewed towards low values (Figure 1b). Uranium concentrations in zircon have a median value of 252 ppm and 25th and 75th percentile values of 98 ppm and 616 ppm, respectively. Log-normalized U concentrations are approximately normally distributed (Figure 1c).

The Th/U ratios of igneous zircon range from <0.01 to 20 (Figure 1d) with a median value of 0.68 and 25th and 75th percentile values of 0.49 and 0.98, respectively. The distribution of Th/U ratios in igneous zircon is more symmetrical around the median than data for metamorphic zircon. Thorium concentrations of igneous zircon have a median value of 125 ppm and 25th and 75th percentile values of 73 ppm and 222 ppm, respectively (Figure 1e). Unlike the distribution for metamorphic zircon (Figure 1b), Th concentrations in igneous zircon are not highly skewed towards low values (Figure 1b, e). Uranium concentrations of igneous zircon have a median value of 186 ppm and 25th and 75th percentile values of 110 ppm and 332 ppm, respectively (Figure 1f). The distributions of U concentrations in metamorphic and igneous zircon are similar (Figure 1c, f).

3 METHODOLOGY

3.1 Closed system

Forward phase equilibria modelling of an average amphibolite-facies metapelite composition from Ague (1991) is used to determine the proportions and major element compositions of major minerals and melt from the wet solidus (~670°C) up to 950°C, at pressures from 0.5 to 1.2 GPa. Values were calculated in a grid with intervals of 1°C and 0.01 GPa. Additionally, we model two isobaric heating paths at 0.6 and 0.9 GPa and one open-system scenario involving melt loss and isobaric heating at 0.9 GPa from the wet solidus up to 950°C.

Calculations were conducted with THERMOCALC v.3.40 (Powell & Holland, 1988) and with the internally consistent dataset (ds62) of Holland and Powell (2011). Modelling was undertaken in the $MnO–Na_2O–CaO–K_2O–FeO–MgO–Al_2O_3–SiO_2–H_2O–TiO_2–Fe_2O_3$ (MnNCKFMASHTO) chemical system with the activity–composition models of White, Powell, Holland, Johnson, and Green (2014). The amount of H_2O in the bulk composition was adjusted so that the system was just saturated with H_2O at the wet solidus at 0.9 GPa. For the 0.6 GPa isobaric heating path, the amount of H_2O was adjusted so that the system was just saturated with H_2O at the wet solidus at 0.6 GPa. Modelled bulk compositions are summarized in Table 1. Phases modelled as pure end-members include quartz, rutile, aqueous fluid (H_2O), kyanite and sillimanite. To calculate the Th/U ratio in equilibrated metamorphic zircon, our modelling approach requires: (1) proportions of the major and accessory minerals and melt at each *P–T* condition, (2) partition coefficients of Th and U between melt and the major and accessory minerals at each *P–T* condition, (3) concentrations of Zr, LREE, P_2O_5, Th and U in the system.

Accessory mineral behaviour is calculated following the methodology of Kelsey et al. (2008) and are discussed in detail elsewhere (Kelsey, Clark, & Hand, 2008; Yakymchuk & Brown, 2014b; Yakymchuk, 2017; Yakymchuk, Clark, & White, 2017). Briefly, melt compositions extracted from THERMOCALC are combined with the solubility expressions for zircon (Boehnke et al., 2013), monazite (Stepanov et al., 2012) and apatite (Wolf & London, 1994) to determine the saturation concentrations of Zr, LREE and P_2O_5 at various *P*–*T* conditions. Because melt compositions across the phase diagram are peraluminous with ASI (molar $Al_2O_3/[Na_2O + K_2O + CaO]$) values greater than 1.1—with the exception of the high-*P* and low-*T* portion of the diagram (c.f. Yakymchuk, 2017)—we use the apatite solubility expression of Wolf and London (1994) instead of other published expressions that were calibrated for metaluminous and peralkaline melt compositions (e.g. Harrison & Watson, 1984). For the high-*P* and low-*T* portion of the diagram, modelled melt composition have ASI values less than 1.1 and the solubility expression of Wolf and London (1994) is not valid. Therefore, we assume that apatite is unreactive at these *P*–*T* conditions.

Assumed bulk rock compositions of Zr, LREE and P are then combined with the solubility expressions for zircon, monazite, and apatite along with stoichiometric concentrations of these elements in accessory minerals and the proportion of melt in the system (estimated from THERMOCALC) to determine the amount of accessory mineral dissolution necessary to saturate the anatectic melt in these elements. We use stoichiometric values of Zr in zircon (497,664 ppm; Kelsey et al., 2008) and P_2O_5 in apatite (41 wt.%; the average of apatite compositions reported in Webster & Piccoli, 2015). For monazite, we start with a stoichiometric concentration of 566,794 ppm LREE (Kelsey et al., 2008) at the solidus, but this is adjusted based on the calculated amount of Th in monazite above the solidus. Throughout, we assume that the atomic weight of the LREE in monazite is 140 g/mol.

Weight fractions of accessory minerals at the solidus are determined from the bulk rock concentrations and stoichiometric values of Zr, P and LREE. At the solidus, all Zr is assumed to reside in zircon, all LREE is in monazite, and any P not allocated to form stoichiometric monazite ($LREEPO_4$) resides in apatite. The concentration of LREE in apatite is determined by partitioning with anatectic melt and a $D_{ap/melt}^{LREE}$ value of 10 is used (e.g. Prowatke & Klemme, 2006). Apatite is assumed to have no

LREE at the solidus. Above the solidus, the amount of LREE in apatite is subtracted from the bulk rock composition and the remainder is used to calculate the mode of monazite and this process is done iteratively to determine the amount of LREE and P allocated to form monazite and apatite (e.g. Yakymchuk, 2017). No adjustment was made to the Ca concentration of the modelled metapelite composition to account for apatite.

Monazite solubility is a function of temperature, pressure, melt composition and the Th concentration of monazite (Stepanov et al., 2012). The concentration of Th in monazite is determined by partitioning with melt. Partitioning of Th into monazite also decreases the saturation concentration of LREE of the melt in monazite-bearing systems (e.g. Stepanov et al., 2012). The concentration of Th in monazite and the concentration of LREE in monazite-saturated melt are calculated iteratively at each *P*–*T* condition (e.g. Yakymchuk, 2017). At very low monazite modes at temperatures just below monazite exhaustion, the modelling here predicts unrealistically high concentrations of ThO_2 (>30 wt.%) in monazite. Therefore, we set a minimum X_{LREE} value of 0.7, where X_{LREE} represents the molar ratio of the LREE to other cations (Th in the modelling here) in monazite (Stepanov et al., 2012). Thorium and U are treated as trace elements and not as essential structural constituents (e.g. Sun & Hanson, 1975) of the accessory minerals. Therefore, their concentrations in anatectic melt are determined by partition coefficients between these elements and the modes of the major and accessory minerals. At each modelled *P*–*T* point, the proportions of the major minerals and melt (calculated by THERMOCALC) and the weight fraction of the accessory minerals are coupled with mineral/melt partition coefficients of Th and U and the concentrations of Th and U in the system (e.g. bulk rock compositions) to determine the concentrations of Th and U in the melt using a batch melting model (e.g. Shaw, 1970; Hanson, 1978). Concentrations of Th and U in minerals are determined from the mineral/melt partition coefficients and the calculated concentrations of Th and U in melt. The proportions of Th and U in the system hosted by the different phases are calculated by combining phase proportions with the calculated concentrations of Th and U in each phase.

Partition coefficients for Th and U used in the modelling for the major minerals and apatite as well as U for monazite are listed in Table 2. Partition coefficients for Th and U between zircon and anatectic melt are a function of temperature and we use the partitioning expressions of Kirkland et al. (2015) to model the Th and U concentrations and Th/U ratios of zircon that is in equilibrium with anatectic melt. For U partitioning between monazite and melt, we use a value of 83, which is an average of the values reported in Stepanov et al. (2012).

For monazite, partition coefficients of Th are highly variable between studies of natural samples and experiments. Figure 2 is a compilation of Th concentrations of coexisting (assumed equilibrated) monazite and melt from experiments and studies of volcanic rocks, S-type granites, nanogranites and leucosomes in migmatites. Glasses from experimental studies have Th concentrations mostly ranging from 100 to 1,000 ppm (Hermann & Rubatto, 2009; Skora & Blundy, 2010; Stepanov et al., 2012; Xing, Trail, & Watson, 2013) with most estimated monazite–melt partition coefficients between 100 and 1,000 (Figure 2). The measured experimental glass compositions have roughly an order of magnitude more Th than the range of Th concentrations measured in S-type granites (Ayers & Harris, 1997; Inger & Harris, 1993; Sawka & Chappel, 1986; Tartèse & Boulvais, 2010; Villaros, Stevens, Moyen, & Buick, 2009) and leucosomes in metasedimentary migmatites (Korhonen, Saito, Brown, Siddoway, & Day, 2010; Sawyer, 1987; Solar & Brown, 2001). For natural samples, Th concentrations of coexisting (assumed equilibrated) monazite and melt (e.g. granite or leucosome) yield partition coefficients that mostly range from 1,000 to 10,000 (Bea, Pereira, & Stroh, 1994; Breiter, 2016; Förster, 1998; Montel, 1993; Pichavant et al., 1987; Wark & Miller, 1993; Weber, Barbey, Cuney, & Martin, 1985). Acosta-Vigil et al. (2010) reported Th concentrations from monazite associated with nanogranites with a monazite–melt partition coefficient of ~12,000. The Th concentration of volcanic Macusani glass (composition JV2 from Pichavant et al., 1987) paired with the average concentration of Th in monazite from Montel (1993) yields a partition coefficient of ~38,000. Considering the wide range of reported and calculated partition coefficients, we investigate different partition values but use a value for $D_{mnz/melt}^{Th}$ of 5,000 as a baseline, which represents the high-end of values from experimental studies and an approximate median for natural rocks.

Bulk compositions of Zr, LREE and P_2O_5 have important implications for the stability of zircon, monazite and apatite during anatexis (Kelsey et al., 2008; Kelsey & Powell, 2011; Yakymchuk & Brown, 2014b; Yakymchuk, 2017; Yakymchuk et al., 2017). Our modelled baseline scenario uses LREE and Zr whole-rock concentrations of 150 ppm, which is a rough average of concentrations in fine-grained sedimentary rocks and metasedimentary migmatites (Taylor & McLennan, 1985; Yakymchuk & Brown, 2014) and a P_2O_5 concentration of 0.19 wt.%, which is an average of amphibolite-facies metapelites reported in Ague (1991).

We investigate various bulk-rock concentrations of Th and U as well as Th/U ratios. Fine-grained sedimentary rocks have Th/U ratios generally between 3.5 and 5.5 (Taylor & McLennan, 1985). Thorium concentrations mostly range from 5 to 17 ppm and U concentrations vary from 1.5 to 4.0 ppm (Taylor & McLennan, 1985). We use bulk concentrations of 3.5 ppm U and 14 ppm Th (average of <2.0 Ga fine-grained sedimentary rocks) in our baseline scenario.

3.2 Open system

Most migmatites and granulites yield field, petrographic and geochemical evidence for melt loss. The preservation of high-temperature mineral assemblages in metamorphic rocks is consistent with the loss of anatectic melt (e.g. Diener, White, & Powell, 2008; White & Powell, 2002). The geochemistry of many granulites is also consistent with the loss of melt enriched in relatively incompatible elements (e.g. Brown, 2013; Guernina & Sawyer, 2003). The extraction of melt from the anatectic crust has important implications for the stability of accessory minerals (Kelsey et al., 2008; Yakymchuk & Brown, 2014b) and the concentrations of the essential structural constituents of accessory minerals in the residuum (e.g. Rapp et al., 1987). Because open-system behaviour in migmatites is path dependent (e.g. Guevara & Caddick, 2016; Mayne, Moyen, Stevens, & Kaisl Aniemi, 2016) and each rock and *P*–*T* path must be evaluated on a case-by-case basis, we choose to model a simple isobaric heating path at 0.9 GPa from the solidus up to a peak temperature of 950°C and use this to investigate the role of melt loss on the Th/U ratio of suprasolidus metamorphic zircon.

Melt loss is modelled assuming that the system becomes open to melt extraction when the proportion of melt reaches a critical threshold. We choose the 7 vol.% melt connectivity threshold of Rosenberg and Handy (2005), which is a rheological threshold where melt along grain boundaries may become interconnected throughout the rock framework. For the modelling, six-sevenths of the melt are extracted leaving 1 vol.% in the system (e.g. Yakymchuk & Brown, 2014a). This amount of residual melt is consistent with observations of thin films on grain boundaries in migmatites that are interpreted to represent melt pseudomorphs (e.g. Holness & Sawyer, 2008), which suggests that migmatites retain a portion of the melt. The major element chemistry of the melt is calculated by THERMOCALC and the trace element concentrations are calculated from the saturation equations of monazite, zircon and apatite for LREE, Zr and P. Concentrations of Th and U in the melt are calculated by partitioning. After each melt loss event, the new melt-depleted composition is used to model the phase equilibria, accessory mineral modes and Th/U values of zircon for the next segment of the isobaric heating path up to the next melt loss event and so on.

4 RESULTS

The results for the baseline scenario for a closed system are plotted on a *P–T* diagram, which has been contoured using Matlab®. A smoothing filter based on a 3x3 Pascal triangle was applied to the results to generate the plot, which minimizes the influence of very small fields on the contours across the diagram. In addition, closed-system results for two isobaric heating paths (0.6 and 0.9 GPa) and one open-system scenario (0.9 GPa isobaric heating) are presented, but no smoothing filter was applied to these results.

4.1 P–T phase diagram

The *P–T* phase diagram (pseudosection) for the average amphibolite-facies metapelite is shown in Figure 3. The temperature of the solidus ranges from 670°C at 0.5 GPa to ~710°C at 1.2 GPa. Rutile is restricted to relatively high pressures (>1.0 GPa). Ilmenite and plagioclase are stable across the entire modelled *P–T* range. No orthopyroxene is predicted to be stable. A narrow field that represents muscovite breakdown to K-feldspar extends from <680°C at 0.5 GPa to <790°C at 1.2 GPa. Biotite breakdown melting occurs after muscovite exhaustion. At > 0.7 GPa, biotite breaks down to garnet over 100–150°C and biotite is completely consumed by ~850°C. A narrow high-variance field extending from 770°C at 0.5 GPa to 850°C at 0.7 GPa represents the breakdown of biotite to cordierite. After biotite exhaustion, melting proceeds via the consumption of quartz and feldspar. This sequence of melting reactions with increasing temperature is common for most aluminous metasedimentary rocks (e.g. Brown, 2013; Clemens, 2006). The modelled amount of melt in normalized molar percentage (approximately equivalent to vol.%) is shown in Figure 4a. Melt proportion contours have steep positive slopes, which indicates that more melt is generated at lower pressures and that melting can proceed via heating and decompression, assuming closed-system behaviour. The amount of melt produced during open system melting during heating and decompression is significantly less (e.g. Mayne et al., 2016; Yakymchuk & Brown, 2014a).

4.2 Accessory mineral proportions

The amounts of zircon, monazite and apatite dissolution in the system relative to the amount of these minerals at the solidus for the baseline scenario are illustrated in Figure 4b–d. The modelled proportions for each accessory mineral are non-linear up temperature with closer spacing of contours at high-temperature. Zircon and monazite dissolution contours are nearly vertical except in the narrow muscovite–K-feldspar field at low temperatures and the narrow biotite–cordierite field at low pressures and high temperatures where contours are less steeply sloping. Apatite proportions are strongly controlled by the aluminum saturation index (ASI) of the melt (e.g. Wolf & London, 1994) and have positive slopes except at low pressure and high temperature, where they are negatively sloping at *P*–*T* conditions outside the stability field of sillimanite and biotite (Figure 3).

4.3 Th/U in melt and zircon

Concentrations of Th and U as well as the Th/U ratios of melt and zircon across the range of modelled *P*–*T* conditions for the baseline scenario are shown in Figure 5. Concentrations of Th in melt increase up temperature until monazite is exhausted (Figure 5a). The contours are closer spaced at higher *T*, corresponding to an increased rate of dissolution at higher *T*. After monazite exhaustion, Th concentrations decrease up temperature. Concentrations of U in melt decrease up temperature (Figure 5b) and are more sensitive to pressure than Th concentrations. The Th/U ratio of melt increases up temperature until monazite exhaustion, after which it is relatively constant (Figure 5c). At low *P*, the Th/U ratio of melt decreases at temperatures above monazite exhaustion.

The Th concentration of zircon in equilibrium follows the same trend as that of the melt, which includes an increase up temperature and then decreases after monazite exhaustion (Figure 5d). Concentrations of U in zircon decrease up temperature in a non-linear manner (Figure 5e). Contours of the concentration of U in zircon are closer spaced at lower temperatures. Th/U values of zircon follow the same general pattern as the Th/U ratio of melt with a maximum value at the monazite-out boundary. After monazite exhaustion, the Th/U ratio of zircon decreases slightly up temperature (Figure 5f).

The sensitivity of the Th/U ratio of equilibrated zircon to the partition coefficient of Th between monazite and melt, and the bulk concentrations of LREE, U, and Th are presented in Figure 6. Contours on Figure 6 represent the *P*–*T* conditions where the modelled Th/U ratio of zircon is equal to 0.1. A Th/U value of 0.1 has been proposed as a boundary between metamorphic and igneous zircon (e.g. Hoskin & Schaltegger, 2003; Rubatto, 2017), although this Th/U value may not be appropriate as shown by the dataset from Western Australia (Figure 1). A Th/U ratio of 0.1 occurs at lower temperatures for low values of $D^{Th}_{mnz/melt}$ (Figure 6a). For very high $D^{Th}_{mnz/melt}$ values, a Th/U ratio of 0.1 for zircon occurs near the monazite-out field boundary (Figure 6a).

Bulk rock concentrations of LREE are essentially a proxy for the amount of monazite present in the system. For higher bulk concentrations of LREE, Th/U ratios of 0.1 of zircon occur at higher temperatures (Figure 6b). For very low concentrations of LREE (e.g. 50 ppm), a Th/U ratio of 0.1 in zircon occurs close to the muscovite-out field boundary. Moderate concentrations of LREE (e.g. 100–200 ppm) result in a Th/U ratio of 0.1 of zircon at lower temperatures than biotite exhaustion at high pressures and close to the biotite–cordierite field at low pressure. For high bulk rock concentrations of LREE (500 ppm) a Th/U ratio of zircon of 0.1 is predicted to occur at UHT conditions.

Low bulk rock concentrations of U or high concentrations of Th result in Th/U ratios of zircon of 0.1 at relatively low temperatures (Figure 6c, d). High bulk rock concentrations of U or low concentrations of Th result in Th/U ratios of 0.1 for zircon at relatively high temperatures (Figure 6c, d). For most modelled bulk rock concentrations of U and Th, a Th/U ratio of 0.1 of zircon occurs between the muscovite-out and biotite-out field boundaries (Figures 3 and 6c, d).

4.4 Isobaric heating paths

Results of the modelling for isobaric heating paths at 0.6 GPa and 0.9 GPa for the baseline scenario are shown in Figures 7 and 8, respectively. The normalized molar proportions of the modelled phases (approximately equivalent to volumetric proportions) are shown in Figures 7a and 8a. Melt production is non-linear with temperature and there are punctuated increases in melt during the breakdown of muscovite at low *T* (Figures 7a and 8a) and at 820°C for the 0.6 GPa heating path due to the breakdown of biotite to cordierite (Figure 7a). The modelled concentration of Th in melt increases with heating and reaches a maximum when monazite is exhausted (Figures 7b and 8b). After monazite is exhausted, the amount of Th in the melt decreases due to dilution. In contrast, the U concentration of the melt decreases along the entire heating path (Figures 7b and 8b). The proportion of each accessory mineral decreases nearly exponentially with increasing temperature and all are completely exhausted by 950°C (Figures 7c and 8c).

The modelled Th budget of the system at the solidus is dominated by monazite (~80%) but decreases with increasing temperature (Figures 7d and 8d). After monazite exhaustion, the melt is the dominant repository of Th (Figures 7d and 8d). In contrast to Th, the U budget of the system at the solidus is nearly equally shared between accessory and major minerals (Figures 7e and 8e). Zircon contains ~30% of the U budget, monazite contains ~20% and apatite ~2% at the solidus. With increasing temperature, the amount of U hosted by the accessory and major minerals decreases with one important exception. For the 0.6 GPa isobaric heating path, the U budget controlled by the major minerals drastically increases at ~800°C (Figure 7e) – this is due to the growth of cordierite, which was modelled with a $D^{U}_{cd/melt}$ value of 1.61 (Bea et al., 1994).

The modelled concentration of ThO_2 in monazite increases with temperature for both heating paths (Figures 7f and 8f). After monazite exhaustion, the concentration of ThO_2 in monazite that would be in equilibrium with the melt decreases during further heating. However, prograde or retrograde monazite growth is not expected because the melt is predicted to be undersaturated in the LREE with respect to monazite above the temperature of monazite exhaustion.

The modelled concentration of U in zircon decreases from >1,000 ppm to <1,000 ppm with increasing temperature (Figures 7g and 8g). With increasing temperature, the modelled concentration of Th in zircon initially decreases from ~200 ppm to ~100 ppm and then increases up to the temperature of monazite exhaustion (Figures 7h and 8h). During heating for both modelled paths, the change of the Th/U ratio of zircon is initially negligible followed by a non-linear increase in the Th/U ratio of zircon until monazite is exhausted. After monazite exhaustion a gentle decrease in the Th/U ratio of zircon is predicted (Figures 7i and 8i).

4.5 Open system

The results for an isobaric heating path at 0.9 GPa in an open system are summarized in Figure 9 along with some of the comparative results for a closed system. The starting composition of the system is the same as the baseline scenario for the closed system. The amount of melt generated in an open system is less than the amount produced in a closed system scenario (Figures 8a and 9a). As a consequence, the accessory minerals are stable to higher temperatures than in the closed system scenario (Figure 9b). Roughly 50% of zircon, 85% of apatite and 25% of monazite are expected to survive heating up to 950°C.

Similar to the closed-system scenario, the modelled concentration of U in melt decreases with heating (Figure 9c). The concentration of U in the system also decreases after each melt loss event because the extracted melt has a higher concentration of U than the residue (Figure 9c). The concentration of Th in the melt increases during the entire heating path (Figure 9d), which contrasts with the decrease after monazite exhaustion in the closed system (Figure 8b). This is due to monazite buffering the Th concentration of melt (and zircon) over the entire heating path. The concentration of Th in the system increases and decreases during the heating path, which is due to the extracted melt having both lower and higher concentrations of Th than the residue at each melt loss event (Figure 9d). The concentration of P_2O_5 in melt increases after 750°C (Figure 9e) when the ASI value of the melt becomes >1.1 and allows apatite dissolution in the modelling.

The predicted concentration of ThO_2 in monazite increases during heating, which is similar to the closed system scenario. Modelled concentrations of U and Th in zircon and the Th/U ratio of zircon are similar between open- and closed-system scenarios for the baseline scenario (Figure 9g–i).

The sensitivity of Th/U ratios of zircon to changes in the bulk rock concentrations of LREE, U and the value of $D_{mnz/melt}^{Th}$ for an open system scenario are investigated in Figure 10. Low bulk rock concentrations of LREE and U result in zircon with higher Th/U ratios (Figure 10a, b). Low values of $D_{mnz/melt}^{Th}$ result in zircon with higher Th/U ratios (Figure 10c). These are similar to the results for the closed system scenario (Figure 6b).

5 DISCUSSION

5.1 Limitations and assumptions of modelling

There are several key assumptions in the modelling, including the following factors: (1) there are no kinetic barriers to the dissolution of accessory minerals, (2) there are no other accessory minerals (e.g. xenotime, allanite) in the system, (3) LREE, Zr and P do not substitute into the major rock-forming minerals, (4) Th substitution in accessory minerals follows Henrian behaviour, (5) rock-wide chemical and thermal equilibration is achieved, (6) apatite is unreactive in the high-*P* and low-*T* portion of the modelled system (i.e. when the ASI value of the modelled melt is <1.1), and (7) no adjustment was made to concentration of Ca in the model metapelite to account for apatite.

First, the modelling assumes that there are no kinetic barriers to dissolution and crystallization during suprasolidus metamorphism. For accessory minerals, the time required to dissolve grains of zircon (Harrison and Watson, 1983), monazite (Harrison & Watson, 1984) and apatite (Rapp & Watson, 1986) are summarized in Figure 11. The dissolution of these phases is sensitive to temperature, the amount of H_2O in the melt and the deviation from saturation (Watson, 1996). For the average metapelite composition modelled here, H_2O concentrations in melt range from ~10 wt.% at the wet solidus down to ~3 wt.% at UHT conditions. There is no significant difference between the H_2O concentration of melt between the open and closed system scenarios. In general, there is not expected to be any significant kinetic barriers to dissolution over orogenic timescales (>1 My). For systems with a realistic 6 wt.% H_2O in the melt, the time required to completely dissolve zircon, monazite and apatite is less than 100 ky to 1 My for the grain sizes considered (Figure 11a–c). In a completely dry system, apatite dissolution may be hindered (Figure 11a). Nonetheless, apatite is not a major contributor to the Th and U budget of the system and is not expected to significantly influence the Th/U ratio of metamorphic zircon.

A second limitation of the modelling is that it does not consider the influence of other accessory minerals that can host significant quantities of Th and U, including allanite and xenotime (e.g. Engi, 2017). However, the modelled composition is representative of an aluminous metapelite at suprasolidus conditions and allanite is not expected to be stable (e.g. Spear, 2010; Wing et al., 2003). Xenotime is a common mineral in subsolidus pelites, but phase equilibria modelling of xenotime and monazite suggests that xenotime is completely consumed at temperatures just above the solidus (Spear & Pyle, 2010), at least in those rock compositions. Xenotime abundance in natural high-temperature granulites is typically lower than monazite and zircon, largely because xenotime and garnet have an inverse abundance relationship (e.g. Spear & Pyle, 2010). Therefore, for the modelled composition and *P–T* conditions, allanite and xenotime are not expected to be stable in the equilibrium assemblage above the solidus. For other compositions, such as Ca-rich metapelites, the influence of allanite on the Th/U ratios of zircon may need to be considered especially at subsolidus conditions (e.g. Finger et al., 2016; Janots et al., 2008). However, subsolidus zircon growth is considered to be much less significant and voluminous than suprasolidus zircon growth.

A third limitation of the modelling is that the essential structural constituents of zircon, monazite and apatite (Zr, LREE and P) are assumed to reside only in the accessory minerals and do not substitute into major minerals. Apatite and monazite are the main repositories of P in suprasolidus metamorphic rocks, but feldspar and garnet can accommodate significant amounts of P (Pyle & Spear, 1999; Villaseca, Martín Romera, De la Rosa, & Barbero, 2003; Kohn & Malloy, 2004; Dumond, Gonclaves, Williams, & Jercinovic, 2015). In most cases, garnet is likely to contain up to a few hundred ppm of P, but extreme concentrations of up to 0.4 wt.% P_2O_5 have been documented in some ultrahigh-temperature metamorphic rocks (Axler & Ague, 2015a, 2015b). In the modelling here, consider a maximum garnet mode of 20 vol.%, and a concentration of 250 ppm P in garnet (e.g. Dumond et al., 2015). A simple mass balance calculation with the apatite and monazite proportions at the solidus will result in garnet hosting ~7% of the P_2O_5 budget. Villaseca et al. (2003) reported concentrations of P_2O_5 in feldspar of 0.18–0.22 wt.%. Considering 20 vol. % feldspar with apatite and monazite modes at the solidus, the result is that feldspar could host 15% of the P_2O_5 budget. In both of these scenarios, the incorporation of

P into major minerals will reduce the *effective concentration* (c.f. Kelsey et al., 2008) of P in the system allocated to form apatite and monazite (e.g. Yakymchuk, 2017), which will result in a slightly decreased stability field of monazite. In the baseline scenario in this study (Figure 5), zircon could therefore attain Th/U ratios >0.1 at slightly lower temperatures if P substitution is considered.

Zirconium can readily substitute into rutile and to a lesser extent into garnet (e.g. Bea et al., 2006; Kohn, Corrie, & Markley, 2015). The substitution of Zr into minerals other than zircon reduces the effective concentration of Zr in the system and results in a reduced stability field of zircon. For example, rutile can accommodate up to a few thousand ppm Zr at UHT conditions (e.g. Tomkins, Powell, & Ellis, 2007). Considering the maximum proportion of rutile in the modelled metapelite composition (~0.2 mol.%), and a concentration of 5,000 ppm Zr in rutile, and a bulk composition of 150 ppm Zr, the result is that ~6% of the bulk rock Zr can be locked in rutile. Garnet can accommodate hundreds of ppm of Zr at UHT conditions, which may be more important. For example, consider an average metapelite with 20 vol.% garnet with an extreme Zr concentration of 100 ppm (e.g. Kohn et al., 2015) and a bulk rock Zr concentration of 150 ppm. The result is that ~11% of the Zr will be locked away in garnet. Again this will slightly reduce the stability field of zircon. However, zircon contains only up to 20% of the U budget of the rock (e.g. Figures 7e and 8e) and a negligible proportion of the Th budget (Figures 7d and 8d). Because of the relatively small influence of zircon on the Th and U concentrations of melt, the role of Zr substitution into major minerals is expected to have a negligible effect on the Th/U ratio of equilibrated zircon.

The impact of LREE substitution into major minerals is potentially more important because the amount of monazite in equilibrium with melt and zircon has a significant impact on the Th budget of the system and the Th/U ratio of equilibrated zircon. In peraluminous migmatites investigated by Bea (1996), feldspar contained roughly 5% of the LREE budget of samples and apatite 10%. The partitioning of LREE into apatite is considered in the models here (e.g. Yakymchuk, 2017) and apatite contains up to 30% of the LREE budget in the modelled accessory minerals. LREE substitution in feldspar is not considered in the models here, but if feldspar contains 20 ppm LREE (the average of values reported in Bea, 1996) and a mode of 20 vol.% (the maximum in the modelling here), this accounts for ~7% of the LREE budget of a rock with a bulk concentration of 150 ppm LREE. The result is a slightly lower effective concentration of LREE allocated to monazite and less monazite will be present in the system to partition Th. Consequently, the modelled Th/U ratio in equilibrated zircon is expected to be slightly higher (e.g. Figure 10a) than for a system where LREE substitution into feldspar is not considered.

The fourth assumption is that concentrations of Th and U in major and accessory minerals can be modelled by partition coefficients and conform to Henry's law. For the major minerals, zircon, and apatite this is likely a valid assumption due to the very low concentrations of Th and U in these minerals. Because Th can substitute into monazite in higher concentration than zircon and apatite, Th partitioning into monazite may depart from Henrian behaviour towards Raoultian behaviour. This has been discussed in detail for experimental results of monazite stability in Skora and Blundy (2010). The consequences for the modelling here are relatively minor because most modelled monazite has low concentrations of Th and Henrian behaviour is likely (Figures 7d and 8d). Modelled ThO_2 concentrations in monazite can reach ~30 wt.% at high temperature (i.e. Th becomes an essential structural constituent in monazite), but this occurs when monazite proportions are approaching zero.

The partition coefficients for Th between monazite and melt vary significantly between experimental studies of natural samples and experiments (Figure 2). Starting compositions of the experimental studies have Th concentrations ranging between 216 and 1063 ppm (Hermann & Rubatto, 2009; Skora & Blundy, 2010; Stepanov et al., 2012; Xing et al., 2013), which are one to two orders of magnitude more than concentrations of Th in most peraluminous granites and metasedimentary rocks. Thorium substitution into monazite may be limited by the substitution mechanism. Direct substitution of tetravalent Th with the formation of vacancies limits the amount of ThO_2 in monazite to ~18 wt.% whereas coupled substitution of Th with Ca can account for up to ~30 wt.% ThO_2 (e.g. Clavier, Podor & Dacheux., 2011). The concentration of Th in monazite from natural samples and experiments have the same general range of values even though the melt compositions are highly variable (Figure 2). Considering the high-Th compositions of the starting materials and melts in experimental studies, we speculate that the amount of Th incorporated into monazite may be limited by these substitution mechanisms and that the partition coefficients derived from co-existing Th-rich melt and monazite in experimental runs may be underestimates.

The fifth assumption of this modelling is that minerals are expected to be in equilibrium with each other (and anatectic melt) and are compositionally homogeneous throughout the rock. In natural systems, most major and accessory minerals preserve some compositional zoning and inclusions are chemically isolated from matrix. Apatite zoning in metamorphic rocks has been documented (e.g. Yang & Rivers, 2002) and chemical zoning in monazite is ubiquitous and used to infer different portions of the metamorphic history (e.g. Engi, 2017; Williams, Jercinovic, & Hetherington, 2007). In suprasolidus metamorphic rocks, zircon that grew from anatectic melt is generally weakly zoned in cathodoluminescence images (e.g. Rubatto, 2017). However, it is clear from studies of REE partitioning between melt, garnet and zircon that equilibrium in trace elements between major and accessory minerals can be a reasonable approximation (e.g. Taylor, Kirkland, & Clark, 2016; Rubatto, 2017). This is the basis for most studies in petrochronology, although there are clear cases where equilibrium was not attained between accessory and major minerals in metamorphic systems (e.g. Lanari & Engi, 2017).

The sixth limitation is that we assume apatite is unreactive when the ASI value of the melt is less than 1.1. Modelled melt ASI values <1.1 are found at < 660°C at 8 kbar and <850°C at 12 kbar (c.f. Yakymchuk, 2017) where melt modes are less than 30 mol.% in closed system (Figure 4a). Apatite is expected to contain a very small portion of the Th and U budgets of the system (e.g. Figures 7d, e and 8d, e) and is expected to have a negligible effect on zircon Th/U ratios in the portion of *P–T* space where we assume apatite is unreactive.

The seventh and final assumption of the modelling is that we do not adjust the concentration of Ca in the bulk system to account for apatite. The amount of Ca that would be needed to be subtracted from the bulk composition to account for apatite is a function of the concentrations of the essential structural constituents of apatite (P) and monazite (LREE, P). For the scenarios presented here, monazite only requires a negligible amount of P (e.g. Yakymchuk, 2017). Approximately 0.25 wt.% of CaO would need to be subtracted from the average metapelite composition at the solidus to account for CaO in apatite, but this amount would vary based on the amount of apatite (and monazite) dissolution in closed- and open-system scenarios. Although slight changes in the phase boundaries are expected, the amount of Th and U in the major phases is relatively small, and this is not expected to have a significant effect on the modelled Th/U ratios in zircon.

5.2 Controls on Th/U ratios of zircon in suprasolidus metamorphic rocks

The modelling here suggests that there are two major controls on the Th/U of zircon in equilibrium with anatectic melt in an average metapelite in closed and open systems. These include: (1) the Th/U ratio and concentrations of Th and U in the system, and (2) the growth and breakdown of monazite.

In an equilibrated system, the concentration of Th and U in the melt is controlled by the modes of the major and accessory minerals, the partition coefficients and the concentrations of Th and U in the system. The concentrations of Th and U in fine-grained sedimentary rocks are variable, but generally have Th/U ratios of 3.5–5.5 (McLennan, Taylor, & Hemming, 2006) with some modern sediments recording extreme values of 1.0 to >6.0 (McLennan & Taylor, 1991). Post-Archean fine-grained sedimentary rocks have U concentrations of around 3.0–3.5ppm and Th concentrations of about 12–16 ppm (Condie, 1993; McLennan et al., 2006). These are also broadly equivalent to the concentrations of these elements in the upper continental crust (e.g. Rudnick & Gao, 2014). However, some pelites can have values that depart from these. Shales with elevated U concentrations, such as those found in reducing environments (e.g. black shales), will generally have low Th/U ratios (e.g. Taylor & McLennan, 1991) and would result in metamorphic zircon with relatively low Th/U ratios. Sediments derived from juvenile sources with low Th/U, such as oceanic island basalts, can be found in back-arc basins (McLennan, Taylor, McCulloch, & Maynard, 1990). Finally, post-depositional leaching of U and/or Th of sedimentary rocks may also contribute to the Th/U of metamorphic zircon.

The breakdown and growth of monazite above the solidus is an important control on Th/U ratios in suprasolidus metamorphic zircon. When melt composition is buffered by monazite, Th partitions mostly between it and anatectic melt (Figures 7d and 8d). Consequently, zircon in equilibrium with monazite and melt will generally have low Th/U ratios. This was proposed in many studies of zircon from high-temperature metapelites and S-type granites (e.g. Cesare et al., 2003; Rubatto et al., 2001; Vavra et al., 1996). As monazite is consumed, the Th concentration of the melt increases (Figures 5a, 7b, 8b and 9d), which results in equilibrated zircon with increasing Th/U values during heating (Figures 7i, 8i and 9i). When monazite is completely exhausted, the Th/U ratio of equilibrated zircon reaches a maximum (Figures 5–10). Because monazite is the primary repository for Th in the modelling here (Figure 7d and 8d), further melting will dilute the melt in Th. Less dilution of U occurs because a larger proportion of U is hosted in the major minerals (Figures 7e and 8e). Consequently, the Th/U ratio of equilibrated zircon decreases after the exhaustion of monazite (Figures 5–10).

This modelling evaluates the composition of zircon in equilibrium with anatectic melt over a range of *P*–*T* conditions, but zircon is generally expected to crystallize during cooling to the solidus (Kelsey et al., 2008; Kohn et al., 2015; Yakymchuk & Brown, 2014b; Yakymchuk et al., 2017). If zircon continuously re-equilibrates its Th/U ratio during cooling to the solidus, then the ratio that is preserved in the zircon will be that at the solidus unless further re-equilibration occurs at subsolidus conditions. However, given the low diffusivity of Th and U in zircon (e.g. Cherniak, Hanchar & Watson, 1997), it is more likely that the zircon will record a range of Th/U values where the cores record early Th/U ratios in the crystallization history and the rims record values near the solidus. This is not explored in the modelling here, but considering that zircon is a relatively minor contributor to the U and Th budget of the system (Figures 7d,e, and 8d, e), the fractionation of Th and U in early grown zircon is not expected to have a major impact on the Th/U ratio of later grown zircon. Nonetheless, a range of Th/U values is expected to be recorded in newly grown anatectic zircon in natural systems.

For the equilibrium closed system scenarios modelled here, the Th/U locked into the zircon is expected to be the value where the retrograde path crosses the wet solidus. For most of the modelled variables, this results in zircon with Th/U ratios <0.1, except at $D^{Th}_{mnz/melt}$ values <3,000 (Figure 6a) or very low concentrations of U (Figure 6c) or very high concentrations of Th (Figure 6d). Migmatites with large proportions of leucosome may reflect approximately closed system behaviour where melt did not escape and these rocks commonly contain metamorphic zircon with Th/U ratios <0.1 (Gasser et al., 2012; Rubatto et al., 2009; Rubatto et al., 2013; Rubatto, 2017). This likely reflects the relatively low temperature of zircon crystallization at or near the wet solidus where zircon Th/U ratios are expected to be <0.1 (Figures 5–8).

In an open system, the extraction of melt elevates the temperature of the solidus (e.g. White & Powell, 2002; White et al., 2007) and the Th/U ratio of the zircon is predicted to be locked in at temperatures higher than the wet solidus. The actual temperature of the solidus will be influenced by the amount of melt extracted from the system, but in the modelling here, it occurs at ~5–20°C below the last melt loss event reached along the modelled isobaric heating path (Figure 10). For all the modelled scenarios, the highest Th/U ratio in zircon is predicted at the solidus for the highest-temperature melt loss event. For most modelled scenarios, UHT conditions are associated with Th/U ratios in zircon >0.1. This is consistent with the results from residual metapelites in the Eastern Ghats (Korhonen et al., 2013), the lower crust in the Ivrea zone (Ewing, Hermann, & Rubatto, 2013; Vavra et al., 1996) and crustal rocks from the Musgrave Province, Central Australia (Howard et al., 2015; Smithies et al., 2011).

The relative timing of monazite and zircon growth during cooling and crystallization of anatectic melt is also an important control in open-system scenarios. Upon cooling, if monazite crystallizes close to the solidus (c.f. Kelsey et al., 2008), initial suprasolidus metamorphic zircon is expected to have high Th/U ratios and late crystallized zircon that grows in the presence of monazite is predicted to have low

Th/U ratios. This is particularly important for rocks with low concentrations of LREE (e.g. Yakymchuk & Brown, 2014b). A similar sequence of Th/U ratios of zircon was documented by Hokada and Harley (2004) in the Napier complex where zircon cores with Th/U> 1 formed during crystallization of the leucosomes and zircon rims with Th/U<1 formed in the presence of monazite late in the crystallization history. In scenarios where zircon and monazite co-precipitate during cooling, such as in systems relatively that are enriched in LREE, then all newly crystallized anatectic zircon is expected to have relatively low Th/U ratios.

5.3 Th/U ratios of zircon in metamorphic rocks

Previous compilations of zircon Th/U ratios have proposed a general threshold Th/U value of 0.1 between metamorphic and igneous zircon (e.g. Hoskin & Schaltegger, 2003; Rubatto, 2017). Based on the new compilation of zircon analyses from Western Australia, it is more appropriate to say that igneous zircon rarely have Th/U < 0.1 and that metamorphic zircon can have values ranging from <0.01 to >10 (Figure 1a). Therefore, zircon with Th/U ratios <0.1 are more likely to be metamorphic and zircon with Th/U ratios >0.1 can be igneous or metamorphic. The results of the modelling here suggest that one of the primary controls on the Th/U ratio of zircon in metamorphic rocks is the presence and proportion of Th-rich monazite. Considering that the database contains zircon from different rock types at various *P*–*T* conditions, the breakdown and growth of other Th-rich minerals may also have a similar influence on the Th budget of the rock and the Th/U ratio of equilibrated zircon.

In rocks with high-Ca bulk compositions (e.g. metabasites and calc-silicate rocks), allanite is a common accessory mineral and is a major repository for Th (Hermann, 2002; Engi, 2017). Allanite is expected to grow from the breakdown of lawsonite and titanite—also relatively Th-rich minerals—during prograde high d*P*/d*T* metamorphism (Spandler, Hermann, Arculus & Mavrogenes, 2003) and also may be partly consumed during high-temperature partial melting (e.g. Klimm, Blundy & Green, 2008). Although the Th/U ratio of equilibrated zircon in these systems will be dependent on the mode of allanite (or other Th-rich minerals), zircon is generally expected to have low Th/U ratios in allanite-bearing systems (Rubatto, 2017).

At subsolidus conditions, the proportion of monazite in metapelites is expected to increase during prograde metamorphism and reach a maximum at the solidus (Spear and Pyle, 2010). While subsolidus prograde zircon growth is not generally expected (c.f. Kohn et al., 2015), any new or recrystallized zircon would be expected to have relatively low Th/U ratios near the solidus and higher Th/U ratios at lower temperatures if there are no additional Th-rich minerals present. In Ca-rich pelites, allanite may be present at lower temperatures than monazite (e.g. Janots et al., 2007; Spear, 2010) and equilibrated zircon is also expected to have relatively low Th/U ratios. However, the Th/U ratio of equilibrated zircon will be significantly influenced by the proportion of Th-rich minerals, which is in part controlled by the bulk composition of the system and the availability of the essential structural constituents of these minerals.

6 CONCLUSIONS

A compilation of metamorphic zircon from Western Australia yields a range of values with a median of 0.4. This median Th/U ratio is higher than 0.1, which is commonly used to separate metamorphic from igneous zircon. Based on phase equilibria modelling, for closed system scenarios, low-temperature crystallization of zircon at or near the wet solidus is likely to lead to Th/U ratios <0.1. However, for open system melting, melt loss will result in elevated solidus temperatures and zircon is predicted to have higher Th/U ratios. Under UHT conditions zircon is expected to have Th/U ratios >0.1. The main controls on the Th/U ratio of suprasolidus metamorphic zircon are (1) the Th/U ratio and concentrations of Th and U in the system, (2) the amount of monazite in the system, which is a function of the concentration of LREE and the amount of melt in the system. Crystallization timing is also likely to be a strong control on zircon grain Th/U ratio; high Th/U ratios are expected early during cooling and melt crystallization in the absence of monazite. By contrast, low Th/U ratios in zircon are expected to occur late in the cooling and crystallization history near the solidus and in the presence of monazite.

ACKNOWLEDGEMENTS

We thank D. Kelsey and G. Dumond for thorough and constructive reviews and D. Robinson for his editorial handling. We also thank M. Brown for many insightful discussions related to this work. The Geological Survey of Western Australia is thanked for making public a wide array of geochemical datasets. CY was partially funded by a National Sciences and Engineering Research Council of Canada Discovery Grant.

REFERENCES

Acosta-Vigil, A., Buick, I., Hermann, J., Cesare, B., Rubatto, D., London, D., & Morgan, G. B. (2010). Mechanisms of Crustal Anatexis: a Geochemical Study of Partially Melted Metapelitic Enclaves and Host Dacite, SE Spain. *Journal of Petrology*, 51, 785–821.

Ague, J. J. (1991). Evidence for major mass transfer and volume strain during regional metamorphism of pelites. *Geology*, 19, 855–858.

Axler, J. A., & Ague, J. J. (2015a). Exsolution of rutile or apatite precipitates surrounding ruptured inclusions in garnet from UHT and UHP rocks. *Journal of Metamorphic Geology*, 33, 829–848.

Axler, J. A., & Ague, J. J. (2015b). Oriented multiphase needles in garnet from ultrahigh-temperature granulites, Connecticut, U.S.A. *American Mineralogist*, 100, 2254–2271.

Ayres, M., & Harris, N. (1997). REE fractionation and Nd-isotope disequilibrium during crustal anatexis: constraints from Himalayan leucogranites. *Chemical Geology*, 139, 249–269.

Bea, F. (1996). Residence of REE, Y, Th and U in Granites and Crustal Protoliths; Implications for the Chemistry of Crustal Melts. *Journal of Petrology*, 37, 521–552.

Bea, F., & Montero, P. (1999). Behavior of accessory phases and redistribution of Zr, REE, Y, Th, and U during metamorphism and partial melting of metapelites in the lower crust: an example from the Kinzigite Formation of Ivrea-Verbano, NW Italy. *Geochimica et Cosmochimica Acta*, 63, 1133–1153.

Bea, F., Pereira, M. D., & Stroh, A. (1994). Mineral/leucosome trace-element partitioning in a peraluminous migmatite (a laser ablation-ICP-MS study). *Chemical Geology*, 117, 291–312.

Bea, F., Montero, P., & Ortega, M. (2006). A LA-ICP-MS evaluation of Zr reservoirs in common crustal rocks: implications for Zr and Hf geochemistry, and zircon-forming processes. *The Canadian Mineralogist*, 44, 693–714.

Boehnke, P., Watson, E. B., Trail, D., Harrison, T. M., & Schmitt, A. K. (2013). Zircon saturation re-revisited. *Chemical Geology*, 351, 324–334.

Breiter, K. (2016). Monazite and zircon as major carriers of Th, U, and Y in peraluminous granites: examples from the Bohemian Massif. *Mineralogy and Petrology*, 110, 767–785.

Brown, M. (2013). Granite: From genesis to emplacement. *Geological Society of America Bulletin*, 125, 1079–1113.

Cesare, B., Gómez-Pugnaire, M. T., & Rubatto, D. (2003). Residence time of S-type anatectic magmas beneath the Neogene Volcanic Province of SE Spain: a zircon and monazite SHRIMP study. *Contributions to Mineralogy and Petrology*, 146, 28–43.

Cherniak, D. J., Hanchar, J. M. & Watson, E. B. (1997). Diffusion of tetravalent cations in zircon. *Contributions to Mineralogy and Petrology*, 127, 383–390.

Clavier, N., Podor, R. & Dacheux, N. (2011). Crystal chemistry of the monazite structure. *Journal of the European Ceramic Society*, 31, 941–976.

Clemens, J. D. (2006). Melting of the continental crust: fluid regimes, melting reactions, and source-rock fertility. In: Brown, M., & Rushmer, T. (eds). Evolution and differentiation of the Continental Crust. Cambridge: Cambridge University Press. pp 296–330.

Condie, K. C. (1993). Chemical composition and evolution of the upper continental crust: Contrasting results from surface samples and shales. *Chemical Geology*, 104, 1–37.

Diener, J. F. A., White, R. W., & Powell, R. (2008). Granulite facies metamorphism and subsolidus fluid-absent reworking, Strangways Range, Arunta Block, central Australia. *Journal of Metamorphic Geology*, 26, 603–622.

Duc-Tin, Q., & Keppler, H. (2015). Monazite and xenotime solubility in granitic melts and the origin of the lanthanide tetrad effect. *Contributions to Mineralogy and Petrology*, 169, 1–26.

Dumond, G., Goncalves, P., Williams, M.L., & Jercinovic, M.J. (2015). Monazite as a monitor of melting, garnet growth and feldspar recrystallization in continental lower crust. *Journal of Metamorphic Geology*, 33, 735–762.

Engi, M. (2017). Petrochronology Based on REE-Minerals: Monazite, Allanite, Xenotime, Apatite. *Reviews in Mineralogy and Geochemistry*, 83, 365–418.

Ewing, T. A., Hermann, J., & Rubatto, D. (2013). The robustness of the Zr-in-rutile and Ti-in-zircon thermometers during high-temperature metamorphism (Ivrea-Verbano Zone, northern Italy). *Contributions to Mineralogy and Petrology*, 165, 757–779.

Finger, F., Krenn, E., Schulz, B., Harlov, D., & Schiller, D. (2016). "Satellite monazites" in polymetamorphic basement rocks of the Alps: Their origin and petrological significance. *American Mineralogist*, 101, 1094–1103.

Förster, H.-J. (1998). The chemical composition of REE-Y-Th-U-rich accessory minerals in peraluminous granites of the Erzgebirge-Fichtelgebirge region, Germany; Part I, The monazite-(Ce)-brabantite solid solution series. *American Mineralogist*, 83, 259–272.

Guernina, S., & Sawyer, E. W. (2003). Large-scale melt-depletion in granulite terranes: an example from the Archean Ashuanipi Subprovince of Quebec. *Journal of Metamorphic Geology*, 21, 181–201.

Guevara, V., & Caddick, M. (2016). Shooting at a moving target: phase equilibria modelling of high ‐ temperature metamorphism. *Journal of Metamorphic Geology*, 34, 209–235.

Hanson, G. N. (1978). The application of trace elements to the petrogenesis of igneous rocks of granitic composition. *Earth and Planetary Science Letters*, 38, 26-43.

Harley, S. L., Kelly, N. M., & Möller, A. (2007). Zircon Behaviour and the Thermal Histories of Mountain Chains. *Elements*, 3, 25–30.

Harrison, T. M., & Watson, E. B. (1983). Kinetics of zircon dissolution and zirconium diffusion in granitic melts of variable water content. *Contributions to Mineralogy and Petrology*, 84, 66–72.

Harrison, T. M., & Watson, E. B. (1984). The behavior of apatite during crustal anatexis: equilibrium and kinetic considerations. *Geochimica et Cosmochimica Acta*, 48, 1467–1477.

Hermann, J. (2002). Allanite: thorium and light rare earth element carrier in subducted crust. *Chemical Geology*, 192, 289–306.

Hermann, J., & Rubatto, D. (2009). Accessory phase control on the trace element signature of sediment melts in subduction zones. *Chemical Geology*, 265, 512–526.

Holland, T. J. B., & Powell, R. (2011). An improved and extended internally consistent thermodynamic dataset for phases of petrological interest, involving a new equation of state for solids. *Journal of Metamorphic Geology*, 29, 333–383.

Hoskin, P. W., & Schaltegger, U. (2003). The composition of zircon and igneous and metamorphic petrogenesis. *Reviews in mineralogy and geochemistry*, 53, 27–62.

Howard, H. M., Smithies, R. H., Kirkland, C. L., Kelsey, D. E., Aitken, A., Wingate, M. T. D., ... Maier, W. D. (2015). The burning heart — The Proterozoic geology and geological evolution of the west Musgrave Region, central Australia. *Gondwana Research*, 27, 64–94.

Inger, S., & Harris, N. (1993). Geochemical Constraints on Leucogranite Magmatism in the Langtang Valley, Nepal Himalaya. *Journal of Petrology*, 34, 345–368.

Janots, E., Engi, M., Berger, A., Allaz, J., Schwarz, J. O., & Spandler, C. (2008). Prograde metamorphic sequence of REE minerals in pelitic rocks of the Central Alps: implications for allanite–monazite–xenotime phase relations from 250 to 610 C. *Journal of Metamorphic Geology*, 26, 509–526.

Johnson, T. E., Clark, C., Taylor, R. J., Santosh, M., & Collins, A. S. (2015). Prograde and retrograde growth of monazite in migmatites: An example from the Nagercoil Block, southern India. *Geoscience Frontiers*, 6, 373–387.

Kelly, N. M., & Harley, S. L. (2005). An integrated microtextural and chemical approach to zircon geochronology: refining the Archaean history of the Napier Complex, east Antarctica. *Contributions to Mineralogy and Petrology*, 149, 57–84.

Kelsey, D. E., Clark, C., & Hand, M. (2008). Thermobarometric modelling of zircon and monazite growth in melt-bearing systems: examples using model metapelitic and metapsammitic granulites. *Journal of Metamorphic Geology*, 26, 199–212.

Kelsey, D. E., & Powell, R. (2011). Progress in linking accessory mineral growth and breakdown to major mineral evolution in metamorphic rocks: a thermodynamic approach in the Na2O-CaO-K2O-FeO-MgO-Al2O3-SiO2-H2O-TiO2-ZrO2 system. *Journal of Metamorphic Geology*, 29, 151–166.

Kelsey, D. E., & Hand, M., (2015). On ultrahigh temperature crustal metamorphism: phase equilibria, trace element thermometry, bulk composition, heat sources, timescales and tectonic settings. Geoscience Frontiers, 6, 311–356.

Kirkland, C. L., Smithies, R. H., Taylor, R. J. M., Evans, N. & McDonald, B. (2015). Zircon Th/U ratios in magmatic environs. *Lithos*, 212, 397–414.

Klemme, S., Günther, D., Hametner, K., Prowatke, S., & Zack, T. (2006). The partitioning of trace elements between ilmenite, ulvospinel, armalcolite and silicate melts with implications for the early differentiation of the moon. *Chemical Geology*, 234, 251–263.

Klemme, S., Prowatke, S., Hametner, K., & Günther, D. (2005). Partitioning of trace elements between rutile and silicate melts: Implications for subduction zones. *Geochimica et Cosmochimica Acta*, 69, 2361–2371.

Klimm, K., Blundy, J. D. & Green, T. H. (2008). Trace Element Partitioning and Accessory Phase Saturation during H2O-Saturated Melting of Basalt with Implications for Subduction Zone Chemical Fluxes. *Journal of Petrology*, 49, 523–553.

Kohn, M. J., Corrie, S. L., & Markley, C. (2015). The fall and rise of metamorphic zircon. *American Mineralogist*, 100, 897–908.

Kohn, M. J., & Malloy, M. A. (2004). Formation of monazite via prograde metamorphic reactions among common silicates: implications for age determinations. *Geochimica et Cosmochimica Acta*, 68, 101–113.

Korhonen, F.J., Clark, C., Brown, M., Bhattacharya, S., & Taylor, R. (2013). How long-lived is ultrahigh temperature (UHT) metamorphism? Constraints from zircon and monazite geochronology in the Eastern Ghats orogenic belt, India. *Precambrian Research*, 234, 322–350.

Korhonen, F. J., Saito, S., Brown, M., Siddoway, C. S., & Day, J. M. D. (2010). Multiple Generations of Granite in the Fosdick Mountains, Marie Byrd Land, West Antarctica: Implications for Polyphase Intracrustal Differentiation in a Continental Margin Setting. *Journal of Petrology*, 51, 627–670.

Lanari, P., & Engi, M. (2017). Local Bulk Composition Effects on Metamorphic Mineral Assemblages. *Reviews in Mineralogy and Geochemistry*, 83, 55–102.

Mahood, G., & Hildreth, W. (1983). Large partition coefficients for trace elements in high-silica rhyolites. *Geochimica et Cosmochimica Acta*, 47, 11–30.

Mayne, M. J., Moyen, J. F., Stevens, G., & Kaisl Aniemi, L. (2016). Rcrust: a tool for calculating path ‐ dependent open system processes and application to melt loss. *Journal of Metamorphic Geology,* 34, 663–682.

McLennan, S. M., & Taylor, S. R. (1991). Sedimentary Rocks and Crustal Evolution: Tectonic Setting and Secular Trends. *The Journal of Geology*, 99, 1–21.

McLennan, S. M., Taylor, S. R., & Hemming, S. R. (2006). Composition, differentiation, and evolution of continental crust: constraints from sedimentary rocks and heat flow. In: Evolution and Differentiation of the Continental Crust (eds Brown, M. & Rushmer, T.). Cambridge: Cambridge University Press. pp 92–134.

McLennan, S. M., Taylor, S. R., McCulloch, M. T., & Maynard, J. B. (1990). Geochemical and Nd-Sr isotopic composition of deep-sea turbidites: Crustal evolution and plate tectonic associations. *Geochimica et Cosmochimica Acta*, 54, 2015–2050.

Montel, J.-M. (1993). A model for monazite/melt equilibrium and application to the generation of granitic magmas. *Chemical Geology*, 110, 127–146.

Nash, W. P., & Crecraft, H. R. (1985). Partition coefficients for trace elements in silicic magmas. *Geochimica et Cosmochimica Acta*, 49, 2309–2322.

Pichavant, M., Herrera, J. V., Boulmier, S., Briqueu, L., Joron, J.-L., Juteau, M., ... Treuil, M. (1987). The Macusani glasses, SE Peru: evidence of chemical fractionation in peraluminous magmas. In: Myson, B.O. (ed.) Magmatic Processes: Physicochemical Principles. University Park, Pennsylvania: Geochemical Society. 359–373,

Powell, R., & Holland, T. J. B. (1988). An internally consistent dataset with uncertainties and correlations: 3. Applications to geobarometry, worked examples and a computer program. *Journal of Metamorphic Geology*, 6, 173–204.

Prowatke, S., & Klemme, S. (2006). Trace element partitioning between apatite and silicate melts. *Geochimica et Cosmochimica Acta*, 70, 4513–4527.

Pyle, J. M., & Spear, F. S. (1999). Yttrium zoning in garnet: coupling of major and accessory phases during metamorphic reactions. *Geological Materials Research*, 1, 1–49.

Rapp, R. P., Ryerson, F., & Miller, C. F. (1987). Experimental evidence bearing on the stability of monazite during crustal anaatexis. *Geophysical Research Letters*, 14, 307–310.

Rapp, R. P., & Watson, E. B. (1986). Monazite solubility and dissolution kinetics: implications for the thorium and light rare earth chemistry of felsic magmas. *Contributions to Mineralogy and Petrology*, 94, 304–316.

Rosenberg, C. L., & Handy, M. R. (2005). Experimental deformation of partially melted granite revisited: implications for the continental crust. *Journal of Metamorphic Geology*, 23, 19–28.

Rubatto, D. (2002). Zircon trace element geochemistry: partitioning with garnet and the link between U–Pb ages and metamorphism. *Chemical Geology*, 184, 123–138.

Rubatto, D. (2017). Zircon: The Metamorphic Mineral. *Reviews in Mineralogy and Geochemistry*, 83, 261–295.

Rubatto, D., & Gebauer, D. (2000). Use of Cathodoluminescence for U-Pb Zircon Dating by Ion Microprobe: Some Examples from the Western Alps. In: *Cathodoluminescence in Geosciences* (eds Pagel, M., Barbin, V., Blanc, P. & Ohnenstetter, D.), pp. 373–400, Springer Berlin Heidelberg, Berlin, Heidelberg.

Rubatto, D., & Hermann, J. (2007). Experimental zircon/melt and zircon/garnet trace element partitioning and implications for the geochronology of crustal rocks. *Chemical Geology*, 241, 38–61.

Rubatto, D., Williams, I. S., & Buick, I. S. (2001). Zircon and monazite response to prograde metamorphism in the Reynolds Range, central Australia. *Contributions to Mineralogy and Petrology*, 140, 458–468.

Rudnick, R. L., & Gao, S. (2014). 4.1 - Composition of the Continental Crust A2 - Holland, Heinrich D. In: *Treatise on Geochemistry (Second Edition)* (ed Turekian, K. K.), pp. 1–51, Elsevier, Oxford.

Sawka, W. N., & Chappell, B. W. (1986). The distribution of radioactive heat production in I‐ and S‐type granites and residual source regions: Implications to high heat flow areas in the Lachlan Fold Belt, Australia. *Australian Journal of Earth Sciences*, 33, 107–118.

Sawyer, E. W. (1987). The Role of Partial Melting and Fractional Crystallization in Determining Discordant Migmatite Leucosome Compositions. *Journal of Petrology*, 28, 445–473.

Schaltegger, U., & Davies, J. H. F. L. (2017). Petrochronology of Zircon and Baddeleyite in Igneous Rocks: Reconstructing Magmatic Processes at High Temporal Resolution. *Reviews in Mineralogy and Geochemistry*, 83, 297–328.

Schaltegger, U., Fanning, C.M., Günther, D., Maurin, J.C., Schulmann, K., & Gebauer, D. (1999). Growth, annealing and recrystallization of zircon and preservation of monazite in high-grade metamorphism: conventional and in-situ U-Pb isotope, cathodoluminescence and microchemical evidence. *Contributions to Mineralogy and Petrology*, 134, 186–201.

Skora, S., & Blundy, J. (2010). High-pressure Hydrous Phase Relations of Radiolarian Clay and Implications for the Involvement of Subducted Sediment in Arc Magmatism. *Journal of Petrology*, 51, 2211–2243.

Skora, S., & Blundy, J. (2012). Monazite solubility in hydrous silicic melts at high pressure conditions relevant to subduction zone metamorphism. *Earth and Planetary Science Letters*, 321, 104–114.

Shaw, D. M. (1970). Trace element fractionation during anatexis. *Geochimica et Cosmochimica Acta*, 34, 237–243.

Solar, G. S., & Brown, M. (2001). Petrogenesis of Migmatites in Maine, USA: Possible Source of Peraluminous Leucogranite in Plutons? *Journal of Petrology*, 42, 789–823.

Smithies, R. H., Howard, H. M., Evins, P. M., Kirkland, C. L., Kelsey, D. E., Hand, M., ... Belousova, E. (2011). High-Temperature Granite Magmatism, Crust–Mantle Interaction and the Mesoproterozoic Intracontinental Evolution of the Musgrave Province, Central Australia. *Journal of Petrology*, 52, 931–958.

Spandler, C., Hermann, J., Arculus, R. & Mavrogenes, J. (2003). Redistribution of trace elements during prograde metamorphism from lawsonite blueschist to eclogite facies; implications for deep subduction-zone processes. *Contributions to Mineralogy and Petrology*, 146, 205–222.

Spear, F. S. (2010). Monazite–allanite phase relations in metapelites. *Chemical Geology*, 279, 55–62.

Spear, F. S., & Pyle, J. M. (2002). Apatite, monazite, and xenotime in metamorphic rocks. *Reviews in Mineralogy and Geochemistry*, 48, 293–335.

Spear, F. S., & Pyle, J. M. (2010). Theoretical modeling of monazite growth in a low-Ca metapelite. *Chemical Geology*, 273, 111–119.

Stepanov, A. S., Hermann, J., Rubatto, D., & Rapp, R. P. (2012). Experimental study of monazite/melt partitioning with implications for the REE, Th and U geochemistry of crustal rocks. *Chemical Geology*, 300, 200–220.

Sun, S. S. & Hanson, G. N. (1975). Origin of Ross Island basanitoids and limitations upon the heterogeneity of mantle sources for alkali basalts and nephelinites. *Contributions to Mineralogy and Petrology*, 52, 77–106.

Tartèse, R., & Boulvais, P. (2010). Differentiation of peraluminous leucogranites "en route" to the surface. *Lithos*, 114, 353–368.

Taylor, R. J. M., Kirkland, C. L., & Clark, C. (2016). Accessories after the facts: Constraining the timing, duration and conditions of high-temperature metamorphic processes. *Lithos*, 264, 239–257.

Taylor, S. R., & McLennan, S. M. (1985). *The Continental Crust: Its composition and evolution*. Oxford: Blackwell Scientific. 312 pp.

Tomkins, H. S., Powell, R., & Ellis, D. J. (2007). The pressure dependence of the zirconium☐in☐rutile thermometer. *Journal of metamorphic Geology*, *25*, 703–713.

Van Westrenen, W., Blundy, J. & Wood, B. (1999). Crystal-chemical controls on trace element partitioning between garnet and anhydrous silicate melt. *American Mineralogist*, 84, 838–847.

Vavra, G., Schmid, R., & Gebauer, D. (1999). Internal morphology, habit and U-Th-Pb microanalysis of amphibolite-to-granulite facies zircons: geochronology of the Ivrea Zone (Southern Alps). *Contributions to Mineralogy and Petrology*, 134, 380–404.

Villaros, A., Stevens, G., Moyen, J.-F., & Buick, I. S. (2009). The trace element compositions of S-type granites: evidence for disequilibrium melting and accessory phase entrainment in the source. *Contributions to Mineralogy and Petrology*, 158, 543–561.

Villaseca, C., Martín Romera, C., De la Rosa, J., & Barbero, L. (2003). Residence and redistribution of REE, Y, Zr, Th and U during granulite-facies metamorphism: behaviour of accessory and major phases in peraluminous granulites of central Spain. *Chemical Geology*, 200, 293–323.

Wark, D. A., & Miller, C. F. (1993). Accessory mineral behavior during differentiation of a granite suite: monazite, xenotime and zircon in the Sweetwater Wash pluton, southeastern California, U.S.A. *Chemical Geology*, 110, 49–67.

Watson, E. B. (1996). Dissolution, growth and survival of zircons during crustal fusion: kinetic principals, geological models and implications for isotopic inheritance. *Earth and Environmental Science Transactions of the Royal Society of Edinburgh*, 87, 43-56.

Weber, C., Barbey, P., Cuney, M., & Martin, H. (1985). Trace element behaviour during migmatization. Evidence for a complex melt-residuum-fluid interaction in the St. Malo migmatitic dome (France). *Contributions to Mineralogy and Petrology*, 90, 52–62.

Webster, J. D., & Piccoli, P. M. (2015). Magmatic apatite: a powerful, yet deceptive, mineral. *Elements*, 11, 177–182.

White, R. W., & Powell, R. (2002). Melt loss and the preservation of granulite facies mineral assemblages. *Journal of Metamorphic Geology*, 20, 621–632.

White, R. W., Powell, R., & Holland, T. J. B. (2007). Progress relating to calculation of partial melting equilibria for metapelites. *Journal of Metamorphic Geology*, 25, 511–527.

White, R.W., Powell, R., Holland, T.J.B., Johnson, T. E., & Green, E.C.R. (2014). New mineral activity–composition relations for thermodynamic calculations in metapelitic systems. *Journal of Metamorphic Geology*, 32, 261–286.

Williams, I. S., & Claesson, S. (1987). Isotopic evidence for the Precambrian provenance and Caledonian metamorphism of high grade paragneisses from the Seve Nappes, Scandinavian Caledonides. *Contributions to Mineralogy and Petrology*, 97, 205–217.

Williams, M. L., Jercinovic, M. J., & Hetherington, C. J. (2007). Microprobe Monazite Geochronology: Understanding Geologic Processes by Integrating Composition and Chronology. *Annual Review of Earth and Planetary Sciences*, 35, 137–175.

Wing, B. A., Ferry, J. M., & Harrison, T. M. (2003). Prograde destruction and formation of monazite and allanite during contact and regional metamorphism of pelites: petrology and geochronology. *Contributions to Mineralogy and Petrology*, 145, 228–250.

Wolf, M. B., & London, D. (1994). Apatite dissolution into peraluminous haplogranitic melts: an experimental study of solubilities and mechanisms. *Geochimica et Cosmochimica Acta*, 58, 4127–4145.

Xing, L., Trail, D., & Watson, E. B. (2013). Th and U partitioning between monazite and felsic melt. *Chemical Geology*, 358, 46–53.

Yakymchuk, C. (2017). Behaviour of apatite during partial melting of metapelites and consequences for prograde suprasolidus monazite growth. *Lithos*, 274–275, 412–426.

Yakymchuk, C., & Brown, M. (2014a). Consequences of open-system melting in tectonics. *Journal of the Geological Society*, 171, 21–40.

Yakymchuk, C. & Brown, M., (2014b). Behaviour of zircon and monazite during crustal melting. *Journal of the Geological Society*, 171, 465–479.

Yakymchuk, C., Clark, C., & White, R. W. (2017). Phase Relations, Reaction Sequences and Petrochronology. *Reviews in Mineralogy and Geochemistry*, 83, 13–53.

Yang, P., & Rivers, T. (2004). The origin of Mn and Y annuli in garnet and the thermal dependence of P in garnet and Y in apatite in calc-pelite and pelite, Gagnon terrane, western Labrador. *American Mineralogist*, 88, 1398–1398.

FIGURE CAPTIONS

FIGURE 1. (a) Th/U ratios of metamorphic zircon from Western Australia. (b) Concentrations of Th in metamorphic zircon from Western Australia. (c) Concentration of U in metamorphic zircon from Western Australia. (d) Th/U ratios of igneous zircon from Western Australia. (e) Concentrations of Th in igneous zircon from Western Australia. (f) Concentration of U in igneous zircon from Western Australia. The inset in each panel is the log-normalized data.

FIGURE 2. Concentration of Th in monazite and melt in experimental glasses and from granites and leucosomes in natural samples. Experimental results from Stepanov et al. (2012) and Xing et al. (2013). Glass compositions from Hermann and Rubatto (2009) are paired with the monazite compositions reported in Skora and Blundy (2010). The Macusani glass composition (JV2 from Pichavant et al., 1987) is paired with the average concentration of Th in monazite from Montel (1993). Nanogranite and paired monazite compositions are from Acosta-Vigil et al. (2010). Monazite and co-existing granite/leucosome are from Förster (1998), Bea et al. (1994), Wark and Miller (1983) Weber et al. (1995) and Breiter (2016). The range of leucosome and peraluminous granite Th concentrations are from Inger and Harris (1993), Villaros et al. (2009), Tartèse and Boulvais (2010), Sawyer (1987), Solar and Brown (2001), and Korhonen et al. (2010).

FIGURE 3. *P–T* phase diagram for an average amphibolite-facies metapelite composition from Ague (1991). The dashed line is the solidus. Mineral abbreviations are from Holland and Powell (2011).

FIGURE 4. (a) Percentage of melt present over the modelled *P–T* range in mol.% (approximately equivalent to vol.%). (b) Percentage of zircon dissolution relative to the amount at the solidus. (c)

Percentage of monazite dissolution relative to the amount at the solidus. (d) Percentage of apatite dissolution relative to the amount at the solidus. The dashed line is the solidus.

FIGURE 5. Th and U concentrations and Th/U ratio of anatectic melt and zircon. Dashed lines are these values outside the stability of zircon in the modelled composition. The thick black lines are the wet solidus in each panel. Abbreviations are apatite (ap), zircon (zrc), and monazite (mnz).

FIGURE 6. Contours of Th/U = 0.1 of zircon for various parameters in the modelling. (a) $D_{mnz/melt}^{Th}$ values ranging from 3,000 to 100,000. Note that values <3,000 do not allow zircon with Th/U<0.1 over the modelled *P–T* conditions for this bulk composition. (b) Bulk rock LREE concentrations ranging from 50–500 ppm, which represents an approximation for the amount of monazite in the system. (c) Bulk rock U concentrations ranging from 2 to 18 ppm for a constant Th concentration of 14 ppm. (d) Bulk rock Th concentrations ranging from 4 to 20 ppm for a constant U concentration of 3.5 ppm.

FIGURE 7. Closed-system isobaric heating path at 0.6 GPa. (a) Normalized molar proportions of major phases. Melt production is non-linear and has two ‘pulses’ of melting at muscovite breakdown at ~700°C and biotite breakdown at ~810°C. (b) Concentrations of Th and U in the melt and residue calculated by mass balance. (c) Percentage of monazite, apatite and zircon remaining during heating. Note that dissolution of all accessory minerals is not linear and is at a faster rate during muscovite and biotite breakdown at ~700°C and ~810°C respectively. (d) Thorium budget of the system. (e) Uranium budget of the system. Monazite and zircon each contain roughly 20–30 wt.% of the U in the system at the solidus. (f) Approximate concentration of ThO_2 (wt.%) in monazite. Thorium content in monazite increases during heating. (g) Concentration of U in zircon in equilibrium with anatectic melt decreases with temperature. (h) Concentration of Th in zircon in equilibrium with melt initially decreases up

temperature and then increases, which reflects the breakdown of monazite. After monazite is depleted at ~845°C, the concentration is no longer buffered by monazite and the concentration of Th in zircon decreases. (i) Th/U ratio of zircon increases during heating and rises above 0.1 at ~800°C. The Th/U ratio of zircon increases until monazite is consumed and then steadily decreases at > 845°C.

FIGURE 8. Closed-system isobaric heating path at 0.9 GPa. (a) Normalized molar proportions of major phases. (b) Concentrations of Th and U in the melt and residue calculated by mass balance. (c) Percentage of monazite, apatite and zircon remaining during heating. (d) Thorium budget of the system. (e) Uranium budget of the system. (f) Approximate concentration of ThO_2 (wt.%) in monazite. Thorium content in monazite increases during heating. (g) Concentration of U in zircon in equilibrium with anatectic melt decreases with temperature. (h) Concentration of Th in zircon in equilibrium with melt initially decreases up temperature and then increases, which reflects the breakdown of monazite. After monazite is depleted at ~840°C, the concentration is no longer buffered by monazite and the concentration of Th in zircon decreases. (i) Th/U ratio of zircon increases during heating and rises above 0.1 at ~770°C. The Th/U ratio of zircon increases until monazite is consumed and then steadily decreases at > 840°C.

FIGURE 9. Open-system isobaric heating path at 0.9 GPa. (a) Normalized molar proportions of major phases. (b) Proportion of accessory minerals remaining relative to the amount at the wet solidus. (c) Concentrations of U (ppm) in the melt, residue and the system calculated by mass balance. (d) Concentrations of Th (ppm) in the melt, residue and the system. (e) Concentrations of P_2O_5 (wt.%) in the melt, residue and the system. (f) Concentration of ThO_2 in monazite. (g) Concentration of U in zircon. (f) Concentration of Th in zircon. (g) Th/U ratio of zircon. The bold dashed line is the wet solidus. ML: melt loss event.

FIGURE 10. Sensitivity of Th/U ratio of zircon in equilibrium with melt to various model parameters for an isobaric heating path at 0.9 GPa in an open system. $LREE_{WR}$: concentration of LREE in the system. U_{WR}: concentration of Uranium in the system. ML: melt loss event. S: solidus for melt loss event number (i.e. S5 is the solidus after ML5).

FIGURE 11. Time required for dissolution of accessory minerals of various diameters and concentrations of H_2O in melt. (a) Zircon (modified from Harrison & Watson, 1983). (b) Monazite (modified from Rapp & Watson, 1986). (c) Apatite (modified from Harrison & Watson, 1984).

SUPPLEMENTARY TABLE S1. Th and U concentration in metamorphic zircon grains.

Table 1. Bulk composition used in phase equilibria modelling (mol.%)

Figures		H_2O	SiO_2	Al_2O_3	CaO	MgO	FeO	K_2O	Na_2O	TiO_2	MnO	O
Closed system												
7	0.6 GPa	5.15	61.23	12.94	1.50	5.24	7.61	2.79	1.90	0.86	0.17	0.61
3–8	0.9 GPa	6.24	60.55	12.80	1.49	5.18	7.52	2.76	1.88	0.85	0.16	0.60
Open system												
9	0.9 GPa, ML1	4.93	60.67	13.13	1.55	5.50	7.98	2.76	1.77	0.90	0.17	0.64
9	0.9 GPa, ML2	3.56	60.80	13.48	1.61	5.84	8.47	2.75	1.67	0.96	0.19	0.68
9	0.9 GPa, ML3	2.32	60.78	13.83	1.67	6.20	8.98	2.73	1.56	1.02	0.20	0.72
9	0.9 GPa, ML4	1.17	60.64	14.17	1.72	6.57	9.52	2.70	1.46	1.08	0.21	0.77
9	0.9 GPa, ML5	0.18	60.33	14.50	1.76	6.96	10.08	2.64	1.37	1.15	0.22	0.82

ML: melt loss event

Table 2. Partition coefficients used in modelling (mineral/melt)

Mineral	Abbreviation	D_U	D_{Th}	Source	Experimental run
Biotite	bi	0.17	1.227	Mahood and Hildreth (1983)	Average
Cordierite	cd	1.61	0.1	Bea et al. (1994)	Average
Garnet	g	0.227	0.1188	van Westrenen et al. (1999)	Average
K-Feldspar	ksp	0.048	0.023	Nash and Crecraft (1985)	Average
Plagioclase	pl	0.093	0.048	Nash and Crecraft (1985)	Average
Quartz	q	0.025	0.08	Nash and Crecraft (1985)	Average
Muscovite	mu	n.d.	n.d.	–	–
Ilmenite	ilm	0.01	0.0027	Klemme et al. (2006)	HD10-1
Rutile	ru	3.8	0.00014	Klemme et al. (2005)	MHD16_1 D
Apatite	ap	0.476	0.733	Prowatke and Klemme (2006)	Average
Zircon	zrc	various	various	Kirkland et al. (2015)	equations (1), (2)
Monazite	mnz	83	various	Stepanov et al. (2012), see text	Average, see text

n.d. = no data

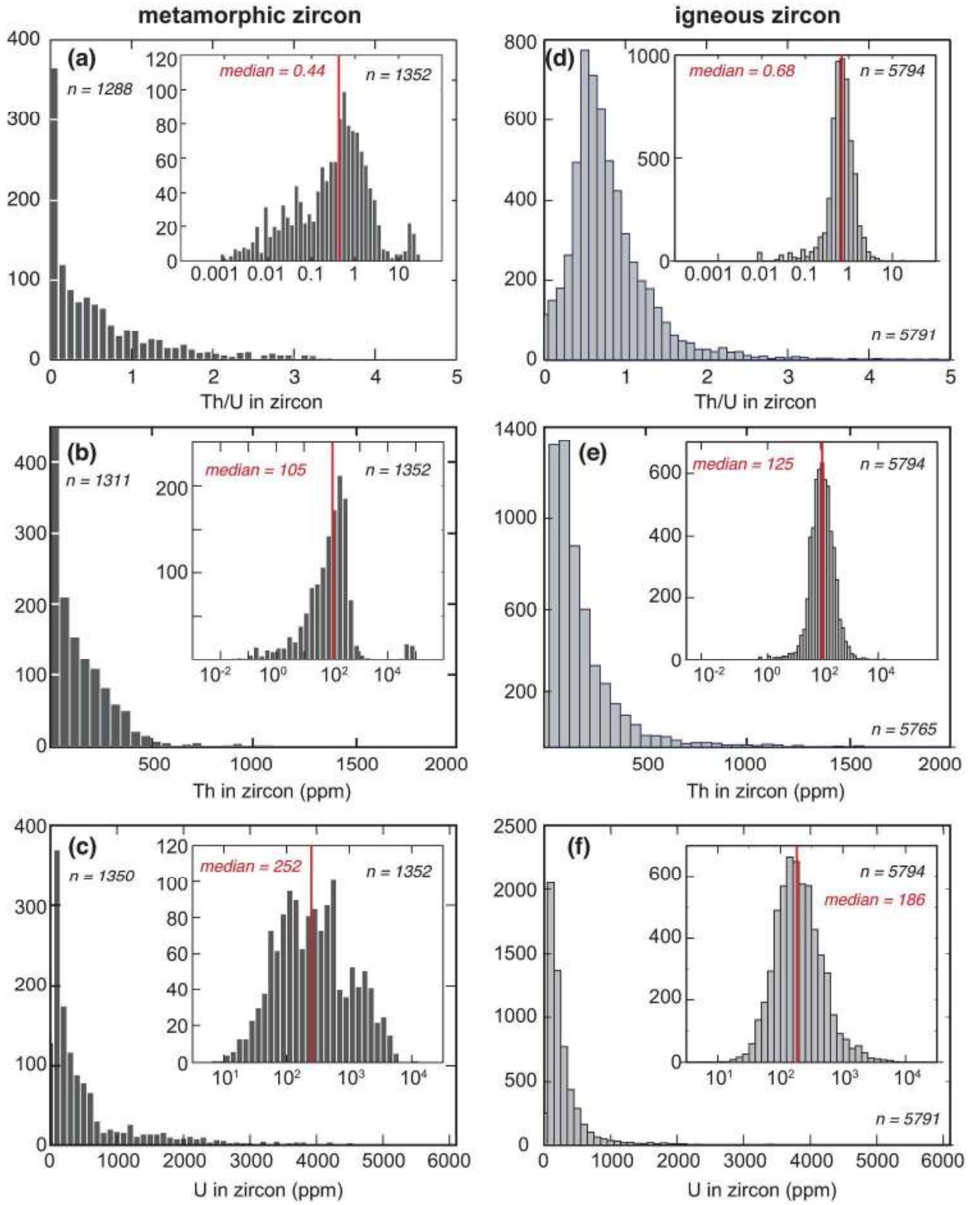

FIGURE 1. (a) Th/U ratios of metamorphic zircon from Western Australia. (b) Concentrations of Th in metamorphic zircon from Western Australia. (c) Concentration of U in metamorphic zircon from Western Australia. (d) Th/U ratios of igneous zircon from Western Australia. (e) Concentrations of Th in igneous zircon from Western Australia. (f) Concentration of U in igneous zircon from Western Australia. The inset in each panel is the log-normalized data.

215x269mm (300 x 300 DPI)

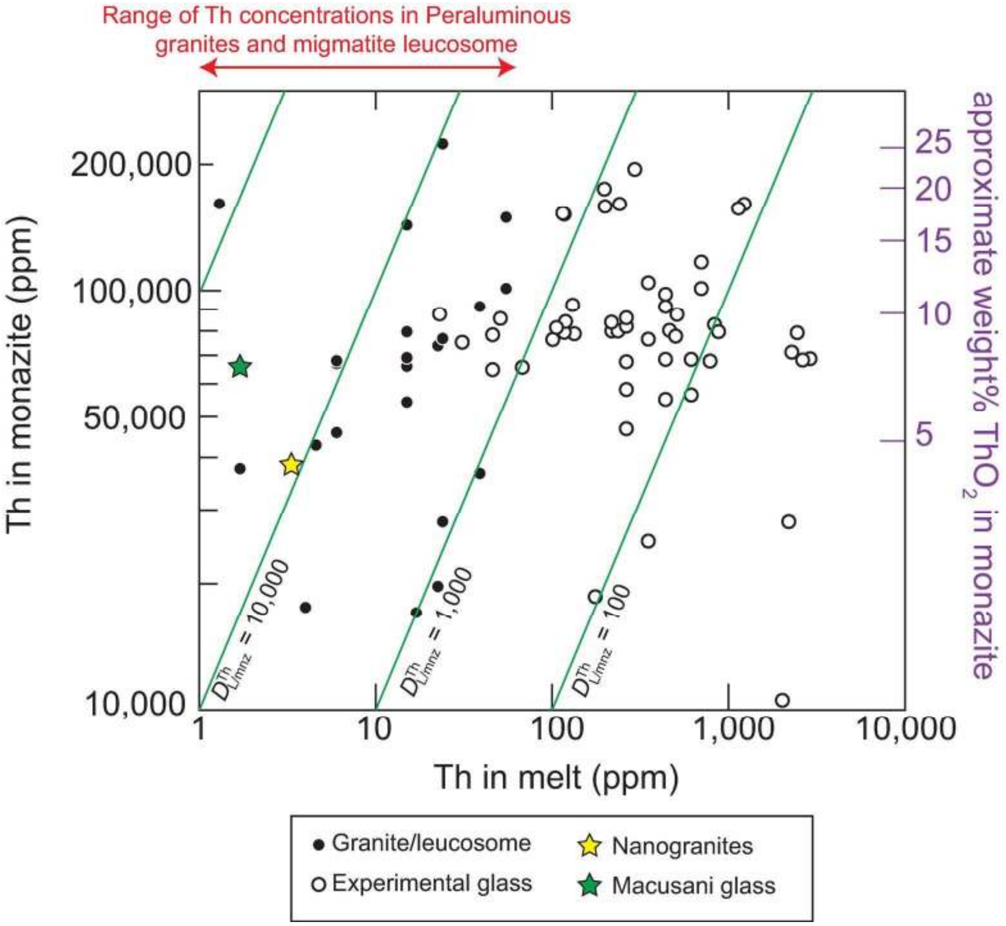

FIGURE 2. Concentration of Th in monazite and melt in experimental glasses and from granites and leucosomes in natural samples. Experimental results from Stepanov et al. (2012) and Xing et al. (2013). Glass compositions from Hermann and Rubatto (2009) are paired with the monazite compositions reported in Skora and Blundy (2010). The Macusani glass composition (JV2 from Pichavant et al., 1987) is paired with the average concentration of Th in monazite from Montel (1993). Nanogranite and paired monazite compositions are from Acosta-Vigil et al. (2010). Monazite and co-existing granite/leucosome are from Förster (1998), Bea et al. (1994), Wark and Miller (1983) Weber et al. (1995) and Breiter (2016). The range of leucosome and peraluminous granite Th concentrations are from Inger and Harris (1993), Villaros et al. (2009), Tartèse and Boulvais (2010), Sawyer (1987), Solar and Brown (2001), and Korhonen et al. (2010).

159x145mm (300 x 300 DPI)

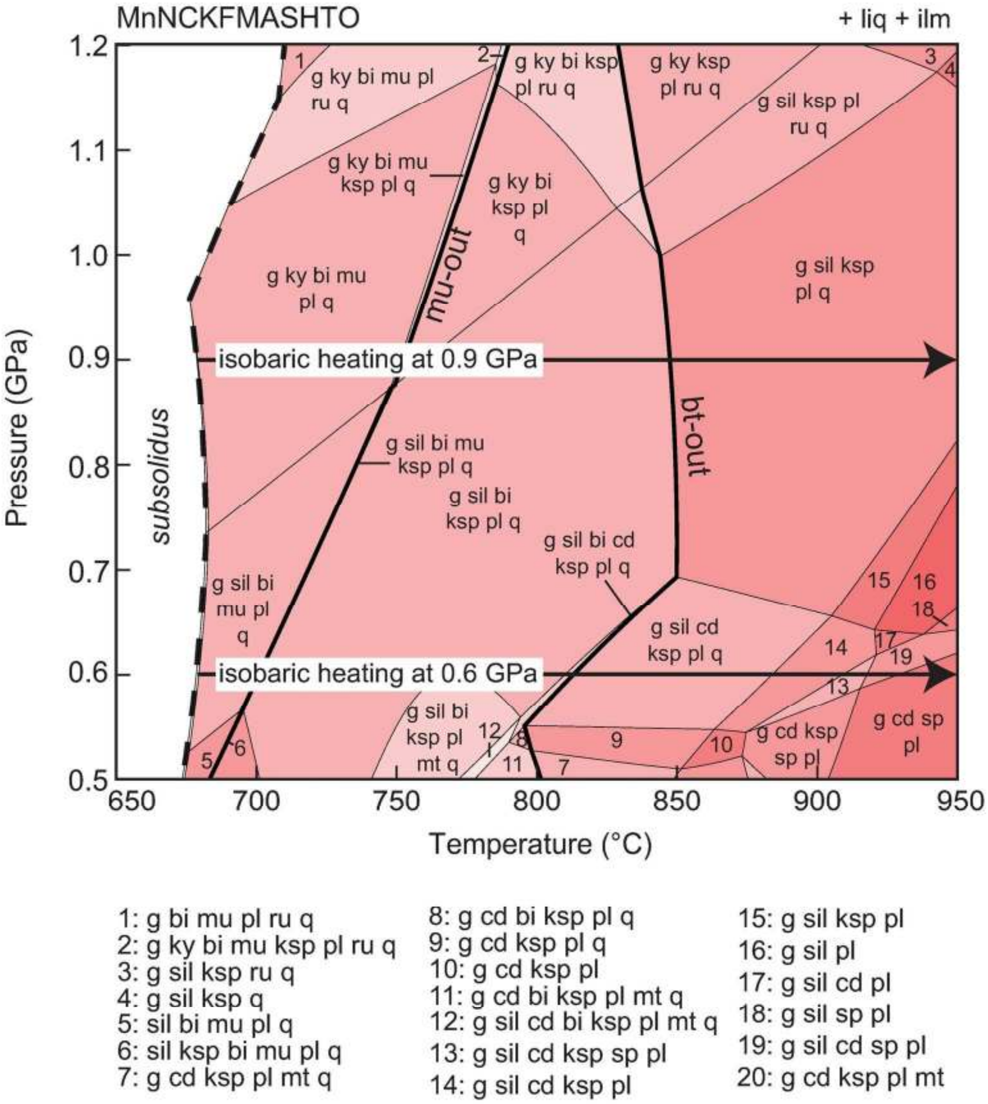

FIGURE 3. P–T phase diagram for an average amphibolite-facies metapelite composition from Ague (1991). The dashed line is the solidus. Mineral abbreviations are from Holland and Powell (2011).

147x162mm (300 x 300 DPI)

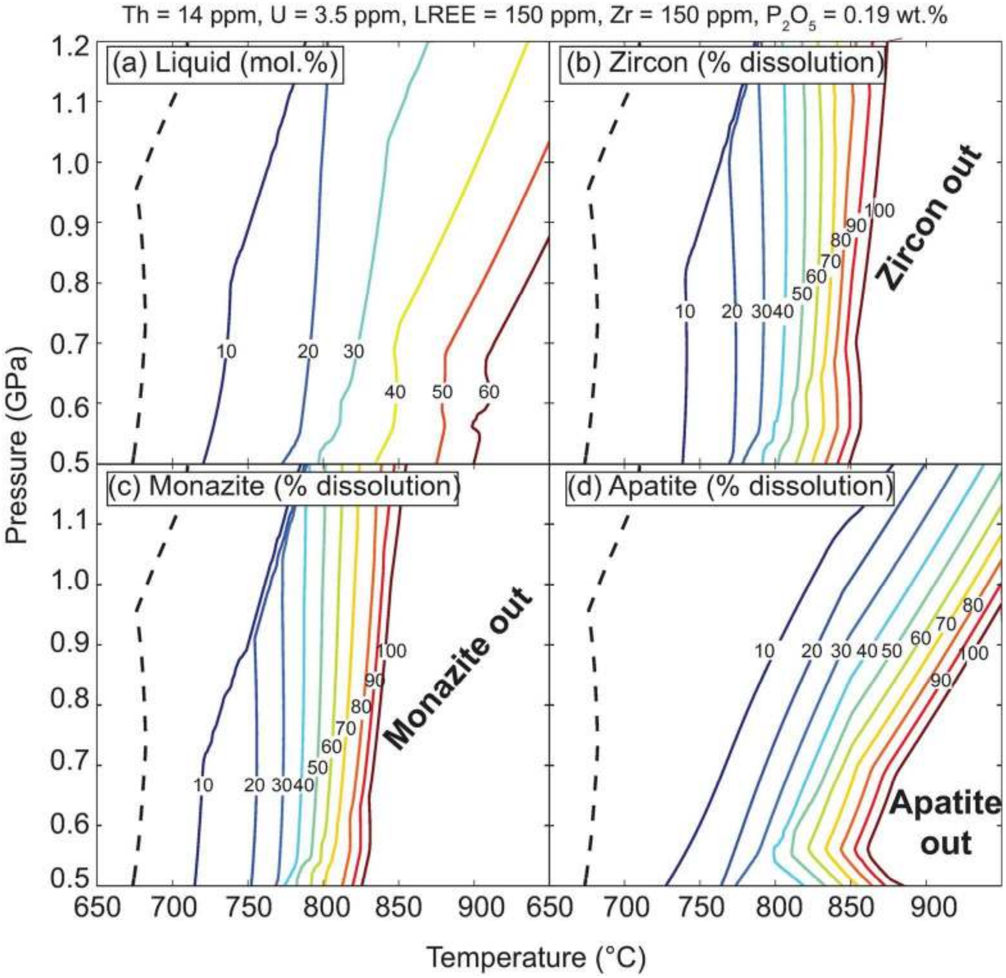

FIGURE 4. (a) Percentage of melt present over the modelled P–T range in mol.% (approximately equivalent to vol.%). (b) Percentage of zircon dissolution relative to the amount at the solidus. (c) Percentage of monazite dissolution relative to the amount at the solidus. (d) Percentage of apatite dissolution relative to the amount at the solidus. The dashed line is the solidus.

143x139mm (300 x 300 DPI)

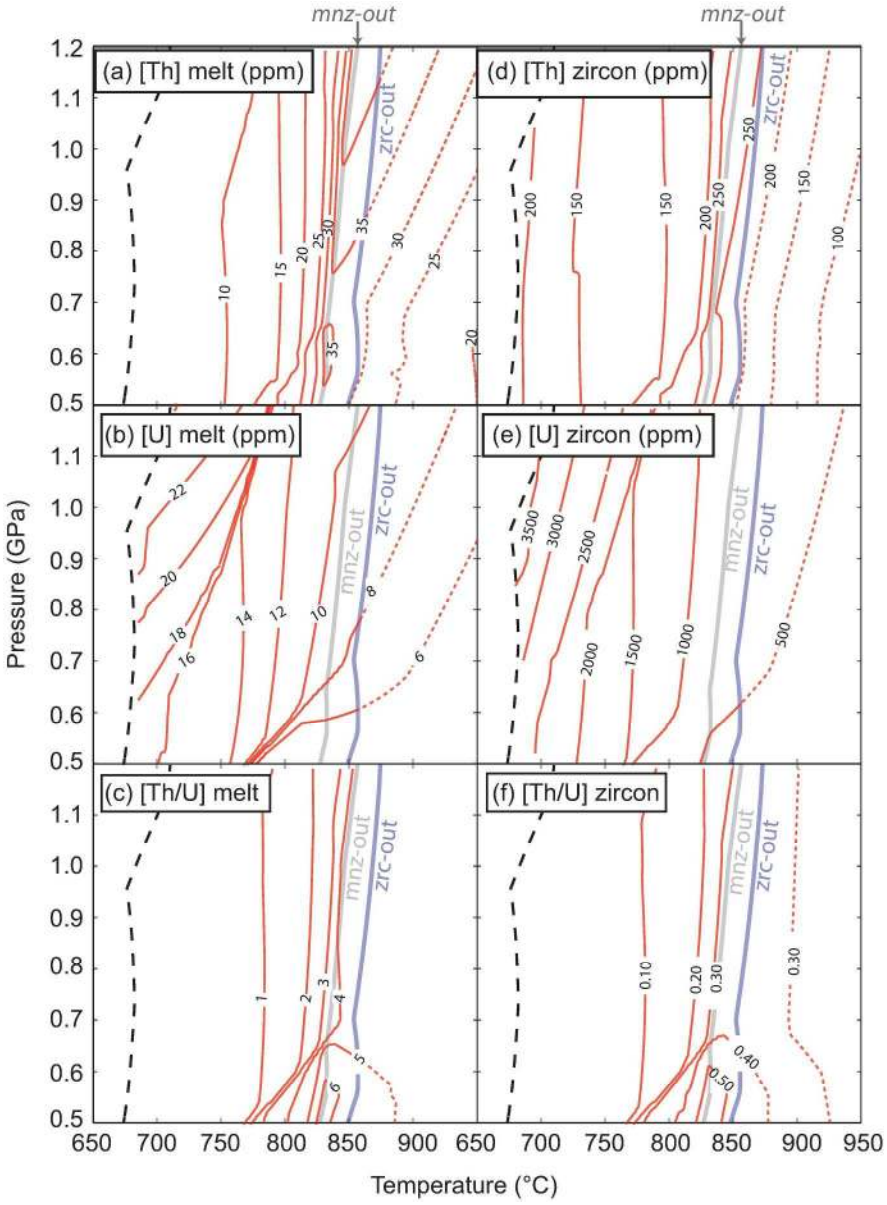

FIGURE 5. Th and U concentrations and Th/U ratio of anatectic melt and zircon. Dashed lines are these values outside the stability of zircon in the modelled composition. The thick black lines are the wet solidus in each panel. Abbreviations are apatite (ap), zircon (zrc), and monazite (mnz).

208x283mm (300 x 300 DPI)

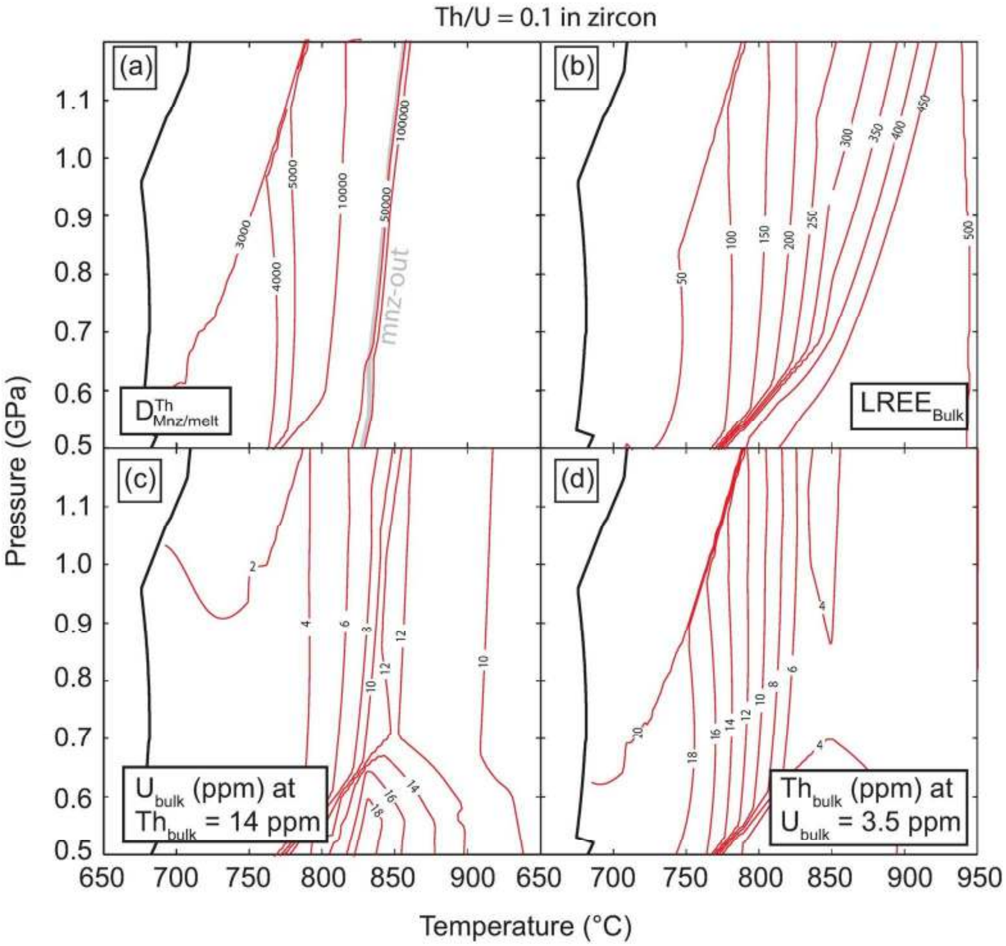

FIGURE 6. Contours of Th/U = 0.1 of zircon for various parameters in the modelling. (a) D_(mnz/melt)^(Th) values ranging from 3,000 to 100,000. Note that values <3,000 do not allow zircon with Th/U<0.1 over the modelled P–T conditions for this bulk composition. (b) Bulk rock LREE concentrations ranging from 50–500 ppm, which represents an approximation for the amount of monazite in the system. (c) Bulk rock U concentrations ranging from 2 to 18 ppm for a constant Th concentration of 14 ppm. (d) Bulk rock Th concentrations ranging from 4 to 20 ppm for a constant U concentration of 3.5 ppm.

144x135mm (300 x 300 DPI)

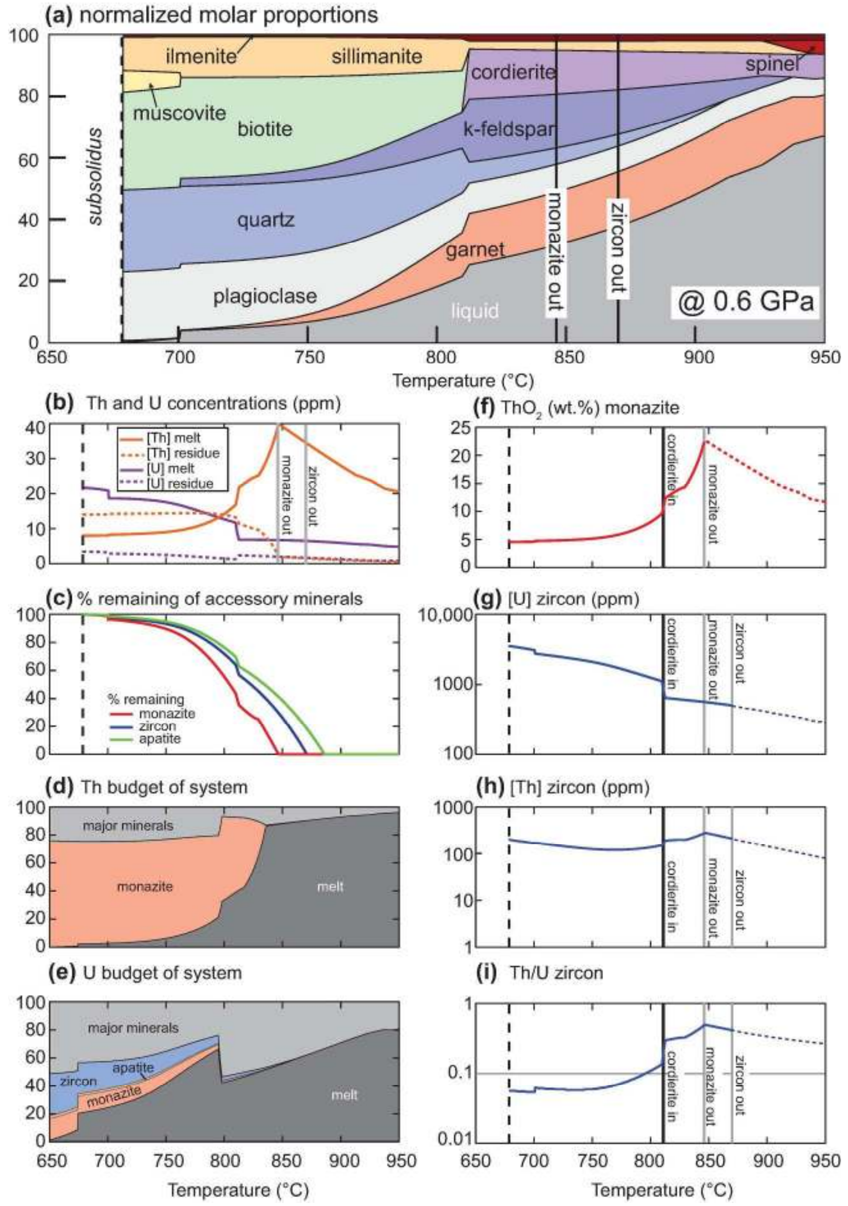

FIGURE 7. Closed-system isobaric heating path at 0.6 GPa. (a) Normalized molar proportions of major phases. Melt production is non-linear and has two 'pulses' of melting at muscovite breakdown at ~700°C and biotite breakdown at ~810°C. (b) Concentrations of Th and U in the melt and residue calculated by mass balance. (c) Percentage of monazite, apatite and zircon remaining during heating. Note that dissolution of all accessory minerals is not linear and is at a faster rate during muscovite and biotite breakdown at ~700°C and ~810°C respectively. (d) Thorium budget of the system. (e) Uranium budget of the system. Monazite and zircon each contain roughly 20–30 wt.% of the U in the system at the solidus. (f) Approximate concentration of ThO2 (wt.%) in monazite. Thorium content in monazite increases during heating. (g) Concentration of U in zircon in equilibrium with anatectic melt decreases with temperature. (h) Concentration of Th in zircon in equilibrium with melt initially decreases up temperature and then increases, which reflects the breakdown of monazite. After monazite is depleted at ~845°C, the concentration is no longer buffered by monazite and the concentration of Th in zircon decreases. (i) Th/U ratio of zircon increases during heating and rises above 0.1 at ~800°C. The Th/U ratio of zircon increases until monazite is

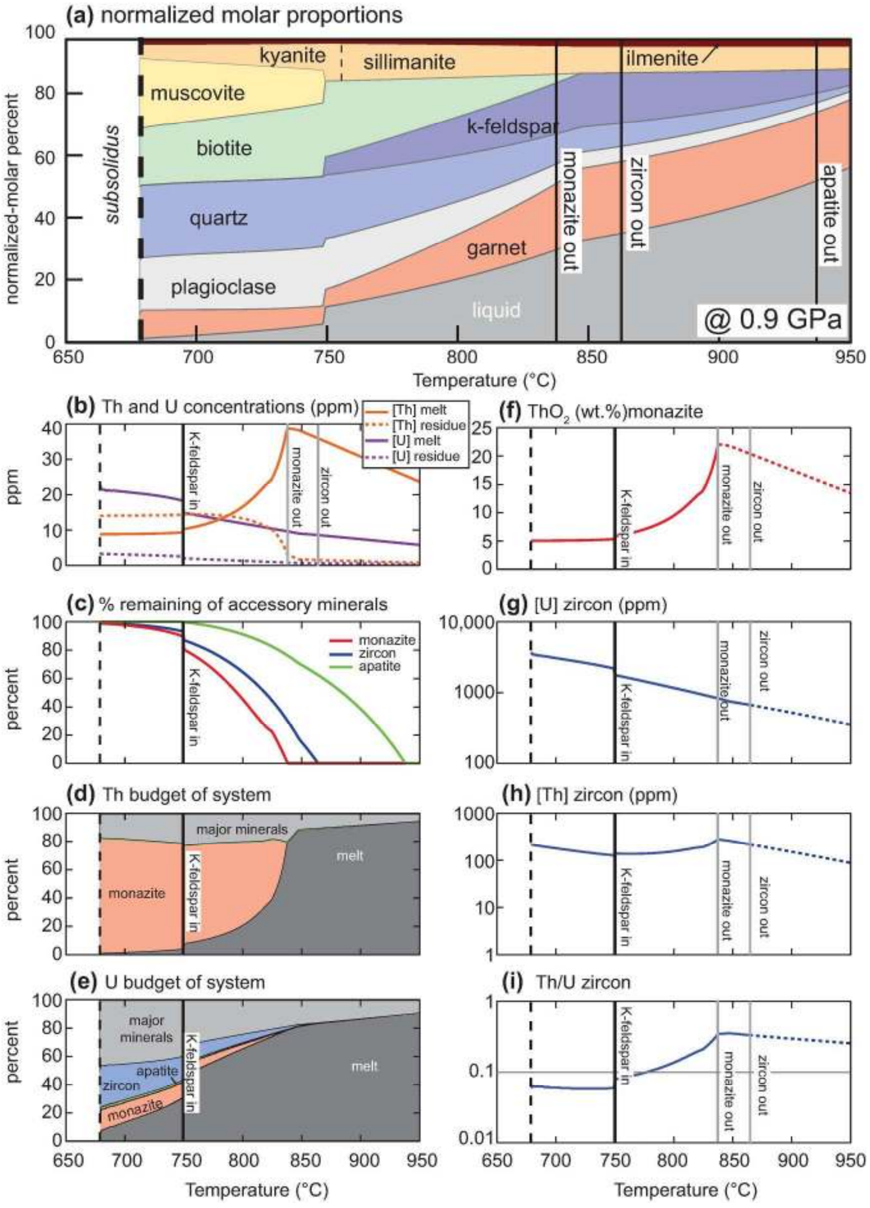

FIGURE 8. Closed-system isobaric heating path at 0.9 GPa. (a) Normalized molar proportions of major phases. (b) Concentrations of Th and U in the melt and residue calculated by mass balance. (c) Percentage of monazite, apatite and zircon remaining during heating. (d) Thorium budget of the system. (e) Uranium budget of the system. (f) Approximate concentration of ThO2 (wt.%) in monazite. Thorium content in monazite increases during heating. (g) Concentration of U in zircon in equilibrium with anatectic melt decreases with temperature. (h) Concentration of Th in zircon in equilibrium with melt initially decreases up temperature and then increases, which reflects the breakdown of monazite. After monazite is depleted at ~840°C, the concentration is no longer buffered by monazite and the concentration of Th in zircon decreases. (i) Th/U ratio of zircon increases during heating and rises above 0.1 at ~770°C. The Th/U ratio of zircon increases until monazite is consumed and then steadily decreases at > 840°C.

181x251mm (300 x 300 DPI)

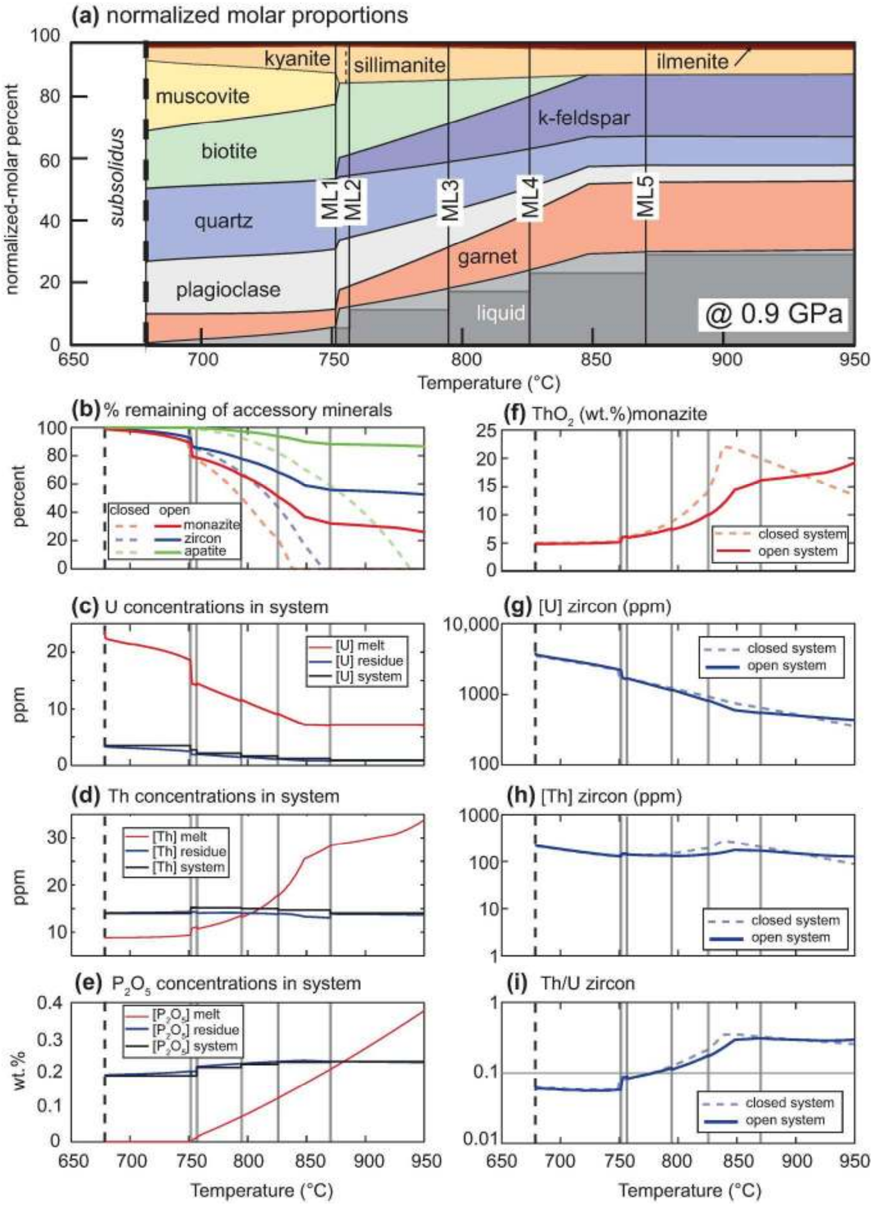

FIGURE 9. Open-system isobaric heating path at 0.9 GPa. (a) Normalized molar proportions of major phases. (b) Proportion of accessory minerals remaining relative to the amount at the wet solidus. (c) Concentrations of U (ppm) in the melt, residue and the system calculated by mass balance. (d) Concentrations of Th (ppm) in the melt, residue and the system. (e) Concentrations of P2O5 (wt.%) in the melt, residue and the system. (f) Concentration of ThO2 in monazite. (g) Concentration of U in zircon. (f) Concentration of Th in zircon. (g) Th/U ratio of zircon. The bold dashed line is the wet solidus. ML: melt loss event.

181x251mm (300 x 300 DPI)

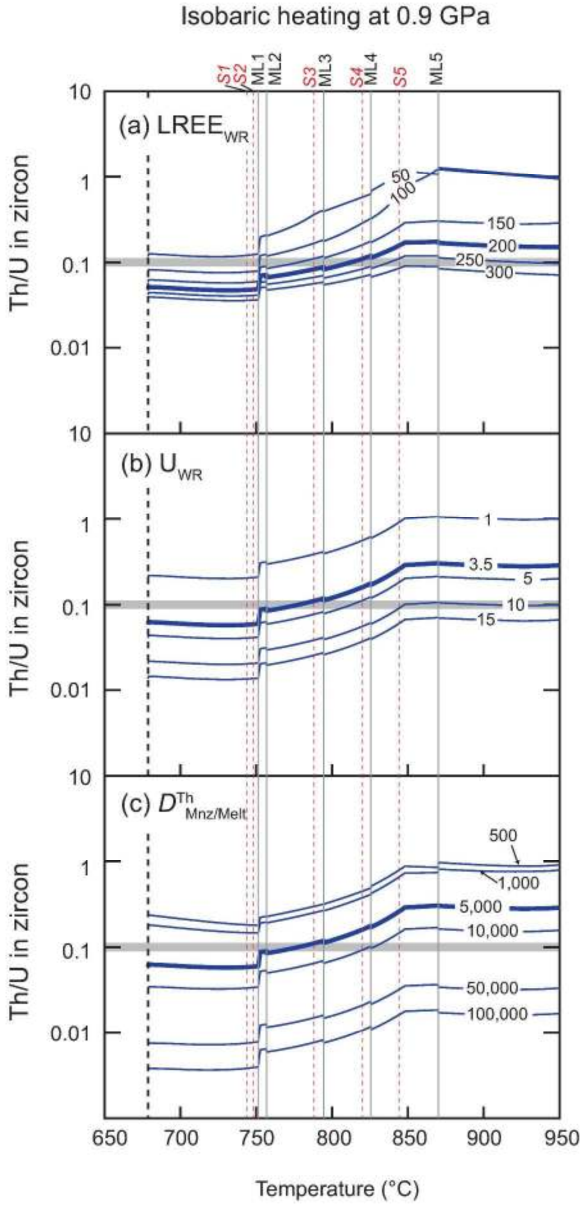

FIGURE 10. Sensitivity of Th/U ratio of zircon in equilibrium with melt to various model parameters for an isobaric heating path at 0.9 GPa in an open system. LREEWR: concentration of LREE in the system. UWR: concentration of Uranium in the system. ML: melt loss event. S: solidus for melt loss event number (i.e. S5 is the solidus after ML5).

198x414mm (300 x 300 DPI)

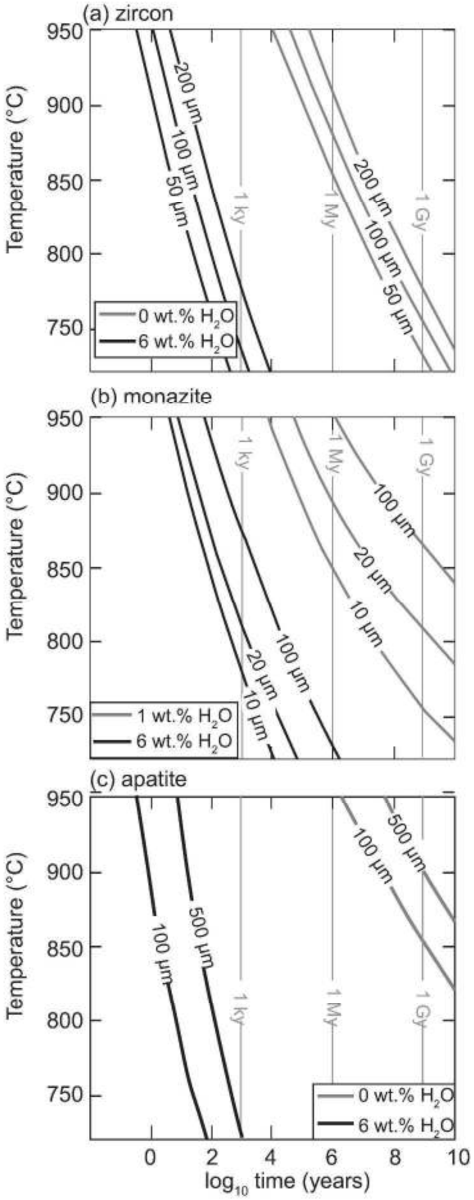

FIGURE 11. Time required for dissolution of accessory minerals of various diameters and concentrations of H2O in melt. (a) Zircon (modified from Harrison & Watson, 1983). (b) Monazite (modified from Rapp & Watson, 1986). (c) Apatite (modified from Harrison & Watson, 1984).

196x505mm (300 x 300 DPI)